Università degli Studi di Ferrara

Università degli Studi di Ferrara

FACOLTÀ DI FISICA E SCIENZE DELLA TERRA
Corso di Laurea in Fisica

Tesi di laurea

CLAS12 RICH Detector: Time Calibration

Candidato:
Alessandro Scarabotto

Relatore:
Prof. Paolo Lenisa

Correlatori:
Dott. Marco Contalbrigo
Dott. Aram Movsisyan

Anno Accademico 2017-2018

A Caro e ai miei genitori

Abstract

Nowadays, Nuclear and High Energy physics are focusing on subatomic particle detection and interaction study. Advanced experiments have been developed to assist challenging requirements by continuously improving technology solutions. Upgrades are always needed to increase precision and accuracy of the experiments, which goes hand by hand with an improvement of the knowledge of the nature around us. Several experimental facilities investigate the subatomic world in different ways.

This Thesis is based on my personal experience at the Thomas Jefferson National Accelerator Facility (TJNAF) in Newport News, Virginia (USA) working with the Ferrara University physics research group. During my academic exchange program at the Old Dominion University in Norfolk, I had the opportunity to join the International research group working at JLab providing my contribution to the current development of innovative particle detectors.

In Chapter 1 the TJNAF which hosts the Continuous Electron Beam Accelerator Facility (CEBAF), will be described. In particular, its focus will lay on CEBAF Large Acceptance Spectrometer (CLAS12) in the experimental Hall B recently enhanced to comply the 12 GeV beam upgrade. An important development of the CLAS12 experiment is correlated to the replacement of one of the already existing gas Cherenkov detectors with an innovative and effective Ring Imaging Cherenkov detector (RICH). This upgrade will improve the hadron identification capabilities over the wider range of momenta and luminosities achieved with the new beam. The CLAS12 RICH detector design will be described in the second part of the chapter.

The second chapter reviews the challenging single photon detection capability. The photosensors chosen for the RICH detector are Multi-Anode Photo-Multiplier Tubes (MAPMTs). A general description of their working principles and performances will be given. The main purpose of this section is to describe how the information from the photodetectors is digitized before being stored on hardware memory for further analysis and studies. This is crucial to really understand the main work of this thesis.

Chapter 3 is devoted to the analysis of the brand new data collected during the 2018 spring run with the TJNAF 10.6 GeV electron beam and a fully operational RICH detector within CLAS12. I supported the Ferrara research group in performing time corrections and calibrations which are critical for increasing precision and accuracy of the RICH measurements. This chapter describes in detail how we addressed data analysis, time offsets and timewalk data features in order to implement an effective correction tool.

Chapter 4 focuses on the analysis of the reconstructed Cherenkov light angle resolution. After applying the time calibration discussed in the third chapter, the angle resolution expected can be studied and compared with expectations. Electrons identified by CLAS12 detectors other than RICH are studied as an independent control sample, useful to estimate RICH performance.

The presented time calibration is crucial to maximize the performance of the RICH detector, designed to greatly enhance the studies on polarized and unpolarized, inclusive, semi inclusive and exclusive deep inelastic scattering of electrons off protons at CLAS12.

Abstract

Al giorno d'oggi, la Fisica Nucleare ad delle Alte Energie si focalizza sullo studio del rilevamento e interazioni di particelle subatomiche. Esperimenti avanzati sono stati sviluppati per assistere gli impegnativi requisiti della Fisica Moderna migliorando continuamente le soluzioni tecnologiche. Gli upgrade sono sempre necessari per migliorare la precisione degli esperimenti, i quali migliorano insieme alla conoscenza della natura intorno a noi. Molti laboratori esplorano il mondo subatomico con diversi metodi.

Questa Tesi si basa sulla mia esperienza personale al Thomas Jefferson National Accelerator Facility (TJNAF) in Newport News, Virginia (USA) dove ho lavorato con un gruppo di ricerca dell'Universit di Ferrara. Durante il mio programma di scambio alla Old Dominion University a Norfolk, ho avuto l'opportunit di unirmi al gruppo internazionale di ricerca al lavoro al JLab contribuendo allo sviluppo di innovativi rilevatori di particelle.

Nel capitolo 1 il TJNAF che ospita il Continuous Electron Beam Accelerator Facility (CEBAF), verr descritto. In particolare, focalizzato sul CEBAF Large Acceptance Spectrometer (CLAS12) nella Hall sperimentale B recentemente migliorato per utilizzare il 12 GeV beam upgrade. Un importante sviluppo dell'esperimento CLAS12 correlato al rimpiazzo di uno degli esistenti gas Cherenkov detectors con un innovativo e efficiente Ring Imaging Cherenkov detector (RICH). Questo upgrade migliorer la capacit di identificare adroni su pi ampio range di momento e luminosit raggiunti dal nuovo fascio. Il design del rilevatore CLAS12 RICH descritto nella seconda parte del capitolo.

Il secondo capitolo descrive il processo di rilevamento a singolo fotone. I fotosensori scelti per il rilevatore RICH sono iMulti-Anode Photo-Multiplier Tubes (MAPMTs). Verranno descritte i loro principi di funzionamento e prestazioni. Lo scopo principale di questa sezione la descrizione di come le informazioni sono digitalizzate dai fotorilevatori prima di essere memorizzate per ulteriori analisi e studi. Questo capitolo cruciale ne comprendere completamente il lavoro dei capitoli successivi.

Il capitolo 3 analizza nuovi dati presi durante la primavera 2018 con un fascio TJNAF di 10.6 GeV e un rilevatore RICH completamente operazionale dentro CLAS12. Ho supportato il gruppo di ricerca di Ferrara producendo una correzione e calibrazione del tempo le quali sono fondamentali per aumentare la precisione di ogni misura con il RICH. Questo capitolo descrive in dettaglio come abbiamo trattato i dati, gli offsets di tempo e la timewalk feature del rilevatore per implementare uno strumento di correzione efficiente.

Il capitolo 4 si focalizza sull'analisi della risoluzione in angolo Cherenkov ricostruito. Dopo aver applicato la calibrazione in tempo discussa nel capitolo 3, la risoluzione in angolo attesa pu essere studiata e paragonata con i dati attesi. Gli elettroni identificati dagli altri rilevatori di CLAS12 sono studiati come un campione indipendente di controllo, utile per stimare le prestazioni del RICH.

La calibrazione in tempo presentata nella tesi cruciale per massimizzare le prestazioni del rilevatore RICH, realizzato per migliorare gli studi sui polarizzati e non polarizzati, inclusive, semi inclusive e exclusive deep inelastic scattering degli elettroni sui protoni per CLAS12.

Contents

List of Figures

Chapter 1

CLAS 12 RICH Detector

Accelerators were invented in the '30s to provide energetic particles to investigate the structure of the atomic nucleus. Since then, they have been used to investigate many aspects of particle physics. Their purpose is to increase the speed and the energy of a beam of particles by generating electric fields that accelerate the particles; and magnetic fields that steer and focus the beam.

The focus of this Thesis will be on Thomas Jefferson National Accelerator Facility (TJNAF) and its advanced experimental equipment. In particular, the Ring Imaging Cherenkov detector (RICH), with its innovative design and components has the role of improving the particle identification capability of the Large Acceptance Spectrometer (CLAS12) hosted in the experimental Hall B. The RICH detector is designed to provide flavor information in deep-inelastic scattering experiments investigating the 3D nucleon structure. This chapter provides an introduction to the Jefferson Lab characteristics, describes the CLAS12 experiment and finally presents the design and purpose of the RICH detector.

1.1 Jefferson Lab

TJNAF, commonly Jefferson Lab (JLab), is one of the United States' National Laboratories, located in Newport News, Virginia. Scientists from all over the world use its particle accelerator, known as the Continuous Electron Beam Accelerator Facility (CEBAF) to study and understand the most basic building blocks of matter and ultimately our world [1].

Specifically the laboratory's mission is to:

- research the atomic nucleus and its fundamental constituents, including precise tests of their interactions;
- apply advanced particle accelerator, detector and other technologies to develop new research capabilities;
- advance knowledge of science and technology through education and public outreach.

Recently, the JLab's expertise developed CEBAF and its experimental equipment with an upgrade which doubled the maximum beam energy to 12 GeV (billion electron volts) with currents up to 100 μA.

CEBAF is a recirculating linac (linear accelerator), with 2 linac sections consisting of 25 cryomodules each (5 added with the new upgrade), see Fig. 1.1. Each cryomodule

is containing 8 superconducting RF cavities (radiofrequency). The total accelerating energy per linac is 1.1 GeV, reaching 2.2 GeV for each loop. The recirculating arcs contain quadrupole and dipole magnets in separate beamlines that enable the beam to be accelerated up to 5 times through both linacs. So at full energy the beam will be available for example at 2.2, 4.4, 6.6, 8.8 or 11 GeV[2].

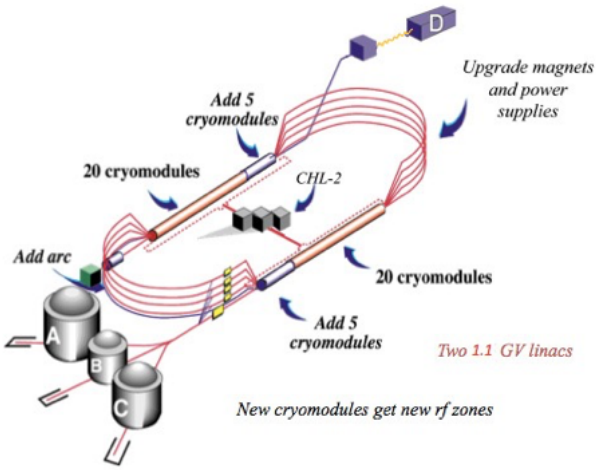

Figure 1.1: Jefferson Lab: 12 GeV Upgrade.

The 2015 NSAC (Nuclear Science Advisory Committee) Long Range Plan clearly announced the importance of this investment: "With the imminent completion of the CEBAF 12 GeV upgrade, its forefront program of using electrons to unfold the quark and gluon structure of hadrons and nuclei and to probe the Standard Model must be realized."

The accelerator electron beam can be simultaneously delivered to the experimental halls at different energies. The 12 GeV electron beam can be converted to 9 GeV photons for experimental Hall D, and up to 11 GeV to halls A, B and C (as mentioned before). Each experimental hall is instrumented with specialized experimental equipment designed to best exploit the features of the CEBAF beam[1].

The detector and data acquisition capabilities at JLab, when coupled with the high-energy electron beams, provide the highest luminosity (10^{39}/eN/cm2/s) capability in the world. Luminosity is the product between beam and target intensity.

1.1.1 Experimental Halls

A brief introduction of the program of each hall follows [3].

Hall A is the largest of these four experimental staging areas. Its physics program spreads from nucleon and few-body form factor studies, strange-quark structure of the proton, nucleon spin and nuclear structure at small inter-nucleon separations. Hall A collaborators represent more than 70 institutions and 18 countries.

Hall B is the site of the upgraded version of the old CLAS (CEBAF Large Acceptance Spectrometer), now called CLAS12, built as part of the JLAB 12 GeV upgrade project. The aim is to investigate and understand nuclear structure via Generalized Parton Distributions (GPD). CLAS12 collaboration involves nearly 150 physicists from more than 30

universities in the U.S., Europe, South America, the former Soviet Union, and Korea.

Hall C will improve the experimental setup adding at the already existing High Momentum Spectrometer a new Super High Momentum Spectrometer (SHMS). Here, the setup supports high-luminosity experiments detecting reaction products with momenta up to the full beam energy, a virtue well matched for making high-precision measurements of neutrino-like cross sections to map valence quarks in nucleons and nuclei.

Hall D searches for new exotic states and strives to measure mass and spin-parity. GlueX is the dedicated spectrometer of this hall. It is designed to search for quantum chromodynamics predicted hybrid mesons using photoproduction via linearly polarized photons. This will allow to run a partial wave analysis of any new observed states to determine whether they have allowed or exotic quantum numbers. The spectrometer can also perform studies of meson and baryon spectroscopy, which bears on the physical origins of quark confinement.

1.2 Hall B: CLAS12

In Hall B, the CEBAF Large Acceptance Spectrometer (CLAS) was designed to study exclusive multi-particle reactions with its advantages of large acceptance and moderate momentum resolution. It has been upgraded to CLAS12 with the 12 Gev upgrade to be optimized for the study of the internal dynamics, 3D imaging of the nucleon, quark hadronization processes through exclusive and semi-inclusive processes. The spectrometer will operate at a luminosity of $10^{35} cm^{-2} s^{-1}$ with highly polarized beam on nucleon targets.

These are the main features of the spectrometer:

- high beam energy and intensity,
- high beam polarization,
- longitudinally and transversely polarized proton and deuterium targets,
- variety of nuclear targets,
- large acceptance, multipurpose spectrometer,
- excellent particle identification.

1.2.1 CLAS12 Design

The detector system consists of two major parts with different functions, the Forward Detector (FD) and the Central Detector (CD)[4].

The Central Detector

The CD is based on a compact superconducting Solenoid magnet with a maximum central magnetic field of 5 Tesla. The Solenoid magnet provides momentum analysis for charged tracks at polar angles from 35^o to 135^o. It also protects the tracking detectors from intense background electrons, and acts as a polarizing field for polarized solid-state targets.

The Forward Detector

The FD detects charged and neutral particles in the polar angle range between 5^o and 40^o. It is based on a 2 T superconducting toroidal magnet and it is organized in 6 sectors

(wedges) to cover the full azimuthal angle extent. It includes a tracking system made of a vertex tracker and three regions of drift chambers (DC), the second of which inside the toroidal field. Baseline particle identification is accomplished by two gas Cherenkov detectors for electron/pion separation (High-Threshold Cherenkov Counter, HTCC, and Low-Threshold Cherenkov Counter, LTCC), a forward Time-Of-Flight (FTOF) system for hadron identification and a preshower and electromagnetic calorimeter to help in electron identification and to detect neutral particles (Fig. 1.2).

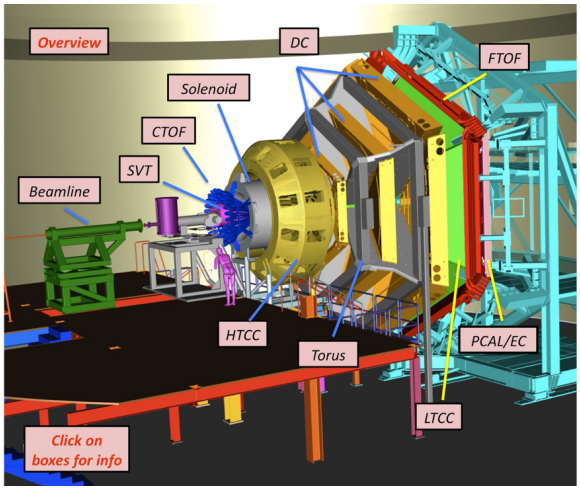

Figure 1.2: Hall B: CLAS12 overview.

For parts of the experimental program the identification of pions and kaons is needed for momenta up to 8 GeV/c. This can be achieved by replacing individual LTCC detectors with Ring Imaging Cherenkov (RICH) detectors. Plans have been developed to build one or more RICH detectors for CLAS12. At the moment only one LTCC sector is replaced by a RICH.

1.3 RICH: Ring Imaging Cherenkov Detector

The existing CLAS detectors as HTCC, LTCC and FTOF were the ones in charge of particle identification for hadrons in the FD, together with the momentum measurements from the drift chambers within the toroidal magnetic field. With only these detectors CLAS12 can not provide adequate kaon identification in the momentum range between 3 and 8 GeV/c. For this goal the RICH detector was built and placed inside Hall B. In Fig. 1.3, it is visible the 3-8 GeV/c momentum gap where the previous detectors have a lack in particle identification resolution.

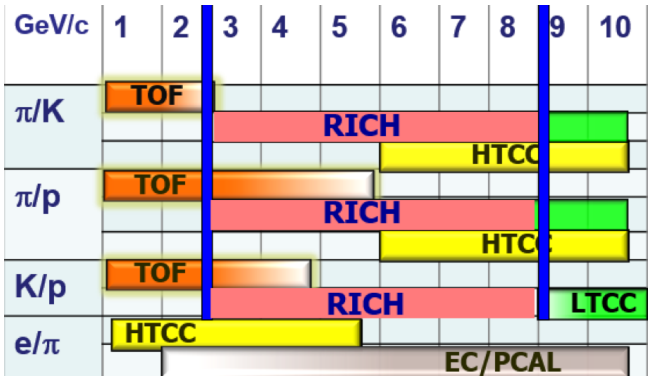

Figure 1.3: CLAS12 particle identification vs momentum range in GeV/c for different detectors.

The RICH detector replaced an individual LTCC detector inside its 6 sectors (wedges) structure. In particular, it is located in sector 4 (on the right) as shown in Fig.1.4. The picture is also reporting the future plans of substituting also sector 1 (on the left) with a RICH detector. In particular, it is located between the torus magnets and the calorimeters (Fig. 1.5).

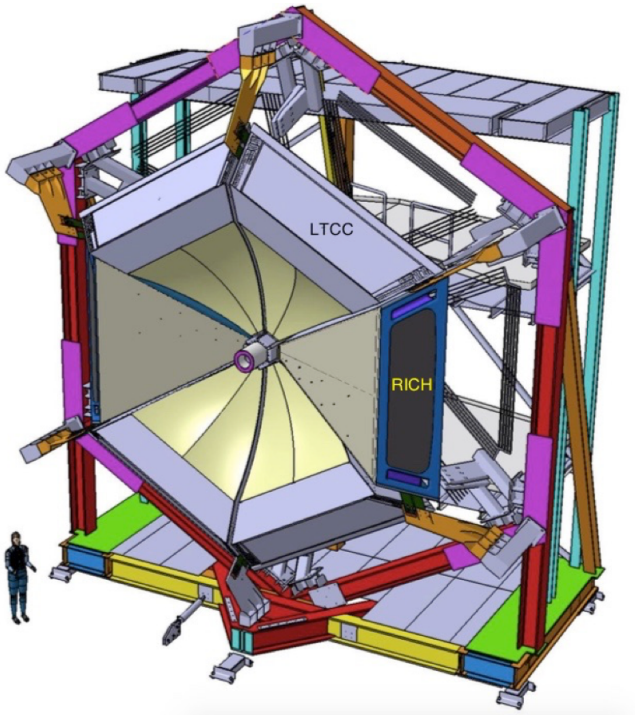

Figure 1.4: RICH position inside the LTCC 6 sectors structure.

.

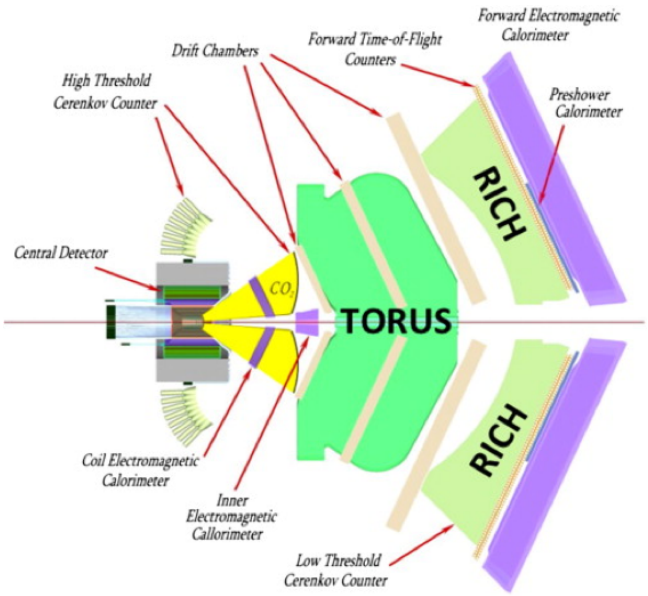

Figure 1.5: RICH detector position inside CLAS12 in Hall B: upper view.

1.3.1 Cherenkov Effect

The Ring Imaging CHerenkov (RICH) detector is based on the so-called Cherenkov light production of a fast particle crossing a medium, typically called radiator. Those photons are emitted from a particle whose velocity β is larger than the velocity of the light in a radiator having refractive index n(λ) depending on the wavelength λ. The light spreads in a cone with opening angle θ_c given by:

$$cos(\theta_c) = \frac{1}{\beta n(\lambda)}$$

After a gap region where the cone opens up, the photons are detected and the ring can be reconstructed (Fig. 1.6). The relation

$$\frac{d^2N}{dLd\lambda} = \frac{2\pi\alpha Z^2}{\lambda^2} sin^2(\theta_c)$$

provides the number of Cherenkov photons emitted per radiator thickness unit L at a given wavelength.

The higher is the number of the detected photos, the more precise is the measurement of the Cherenkov angle. The resolution on position and direction measurements is very important too, considering the error that affects the mapping between photon hit position and emission angle. Then the particle can be identified by its velocity together with the information of the tracking system.

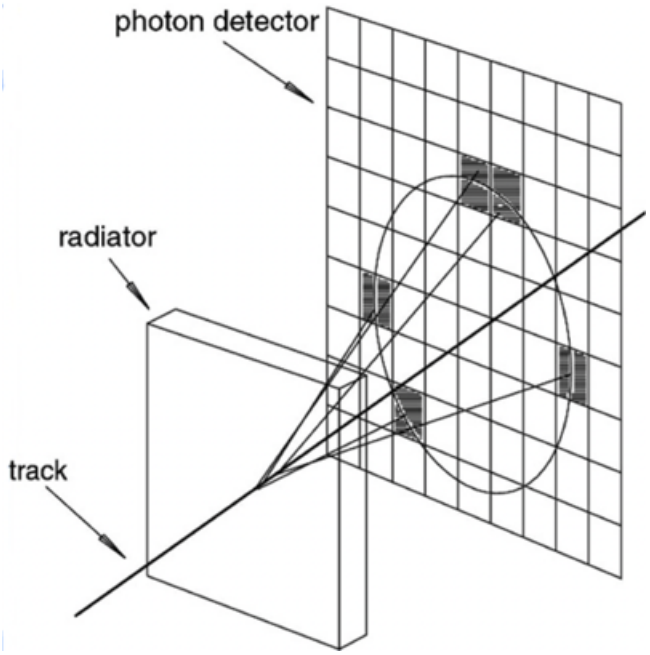

Figure 1.6: Cherenkov effect application.

1.3.2 Scientific Program

In particular, the RICH contributions to the CLAS12 physics program are:

- study of the strange distributions of the nucleon in the valence kinematic region using kaon production in unpolarized and doubly longitudinally polarized deep-inelastic scattering off proton and deuterium targets, as well as exclusive kaon-hyperon and ϕ-meson production;
- study of the flavor and kinematic dependence of the intrinsic transverse quark momenta employing fully differential analyses of pion and kaon production in unpolarized deep-inelastic scattering off proton and deuterium targets;
- study of the TMD quark distributions via the extraction of spin and azimuthal asymmetries for pions and kaons from deep-inelastic scattering off unpolarized, transversely and longitudinally polarized proton and deuterium targets;
- study of the transverse spatial distribution of "valence-like" gluons from hard exclusive ϕ-meson production variety of nuclear targets;
- study of quark propagation through cold nuclear matter via nuclear hadronization and transverse momentum broadening employing pion and kaon production in deep-inelastic scattering off a variety of nuclear targets
- study of exotic meson configurations via the tagging of strangeness- rich final states in quasi-real photoproduction

1.3.3 Design

The RICH geometry design had some constraints regarding the LTCC sectors shape. The external frame has a trapezoidal shape, with a major base of about 4.3 m, an height of about 3.8 m and a depth of about 1 m and it is tilted by 65^o with respect to the vertical axis.

The radiator chosen for the RICH detector is silica aerogel. It is an amorphous solid network of SiO_2 nanosphere with a very low macroscopic density and a refractive index intermediate between gases and liquids which is n=1.05. It offers a low chromatic error and high quantum efficiency in detection of photons in the visible wavelength spectrum.

Multi-Anode Photo-Multipliers Tubes (MAPMTs) were chosen for photodetection. They have high quantum efficiency in the visible and near UV region, give a fast response and provide the necessary spatial resolution. In particular, two devices will compose the active area: flat-panel Hamamatsu H8500 and H12700. They have an active area of 49.0 $\times$ 49.0 mm^2 which comprises an 8 $\times$ 8 array of pixels, each with dimensions 5.8 $\times$ 5.8 mm^2. The choice to have MAPMTs as photon detectors implies to have a total number of about 25000 independent channels.

The detection will happen in two different ways: direct and reflected photons. Forward scattered particles with momenta p = 3 - 8 GeV/c and $\theta < 13^o$ will be imaged directly (Fig. 1.7). The scattered particles with larger angles $13^o < \theta < 35^o$ and lower momenta p = 3 - 6 GeV/c will have a longer path (about 3 times the direct one) to be detected (Fig. 1.8). First they have to be focused by a spherical mirror. Then the geometry force them to pass through a thinner radiator, be reflected by a planar mirror and to cross one last time the aerogel before detection. Inside the sector the environment if filled by nitrogen.

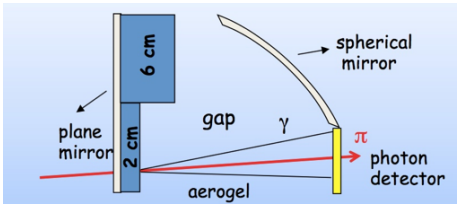

Figure 1.7: Direct Cherenkov light detection.

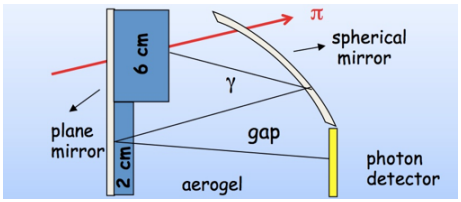

Figure 1.8: Reflected Cherenkov light detection.

This hybrid mirror design is allowing a considerable reduction of the detector's active area (Fig. 1.9). Inside the sector, ten spherical mirrors, placed on top of the photon detector, and seven planar ones, before the aerogel tiles, will contain the photons produced at large angles. Two more planar mirrors will be placed in the inner walls on the sides of the module, not to lose any produced photons. The total area of these mirrors will be about 4 m^2.

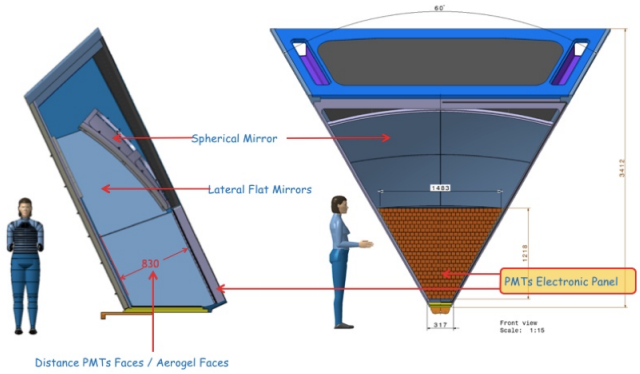

Figure 1.9: Hybrid mirror RICH design for detector's active area reduction.

Chapter 2

RICH Photo-Detectors

Ring Imaging CHerenkov (RICH) detectors are based on the so-called Cherenkov light production. Cherenkov radiation is the phenomenon generated by a particle traveling in a transparent material when its velocity exceeds the speed of light in that medium. It is observed as a cone of light with a specific opening angle, called Cherenkov angle, which can be used to infer the particle identity (mass) when knowing its momentum. In particular, the movement of a charged particle inside a polarizable medium excites the molecules to higher level states. When they return back to the ground state, they re-emit photons as electromagnetic radiation that interfere constructively along a conical wave. The number of photons emitted in this way is very small, so a RICH photon detector has to be sensitive to a single quantum of light. This capability is the main feature of photo-multiplier tubes (PMTs).

2.1 Photo-Multiplier Tubes

2.1.1 PMT

A photomultiplier tube is a vacuum tube consisting of an input window, a photocathode, focusing electrodes, an electron multiplier and an anode usually sealed into an evacuated glass tube. Figure 2.1 shows the schematic construction of a photomultiplier tube [5].

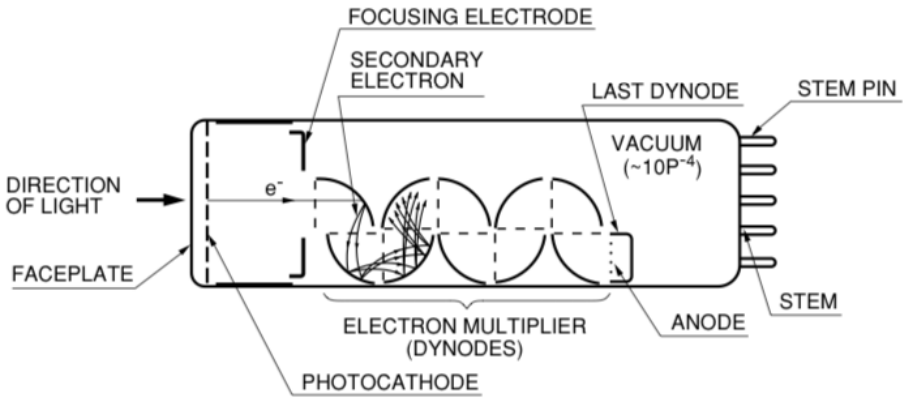

Figure 2.1: Design of a PhotoMultiplier Tube.

Light which enters a photomultiplier tube is detected and produces an output signal through the following processes.

1. Light passes through the input window.

2. Light excites the electrons in the photocathode so that photoelectrons are emitted into the vacuum (external photoelectric effect).

3. Photoelectrons are accelerated and focused by the focusing electrode onto the first dynode where they are multiplied by means of secondary electron emission. This secondary emission is repeated at each of the successive dynodes.

4. The multiplied secondary electrons emitted from the last dynode are finally collected by the anode.

2.1.2 MAPMT

MultiAnode Photomultiplier Tubes (MAPMTs) have been chosen as photon detector for the CLAS12 RICH detector. They are flat panel type multianode PMT assemblies of the H8500 and H12700 Hamamatsu series and feature 52 $\times$ 52 mm^2 area, bialkali photocathode, 8 $\times$ 8 multianode matrix with a 6 mm pixel pitch. The multianode structure has been chosen for the RICH detector to reach the designed position precision of the detected photons. This is required for an effective Cherenkov ring light reconstruction.

Following the sketch in Fig. 2.2, the photoelectrons emitted from the photocathode pass through the focusing mesh and are directed to the first of the metal channel dynodes, then, while being multiplied, they flow to the other dynodes until they reach the multianode structure [6].

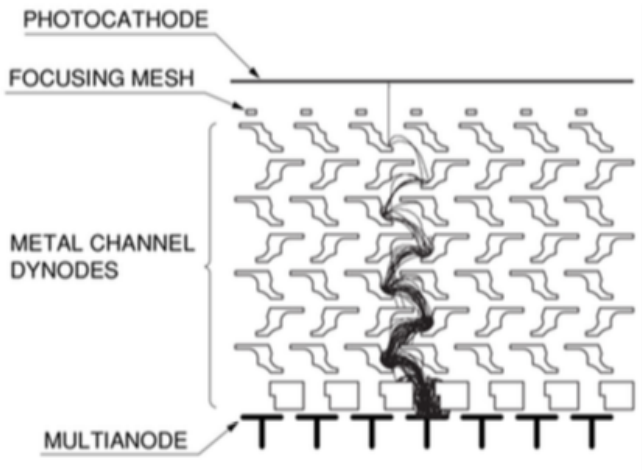

Figure 2.2: MAPMT dynode structure scheme with electron trajectories.

The first sensor model, named H8500 (Fig.2.3), was originally developed for position sensitive scintillation counting in molecular imaging studies (PET and mini-gamma cameras). It features a 49 mm^2 active area with 8 x 8 multianode matrix with a 5.8 mm pixel pitch [7]. Several studies performed on them allowed to validate their use at single photon level. The second sensor model, named H12700 (Fig.2.4), has been lately developed following the demand from high energy physics groups [9] [10]. It features a 48.5 mm^2 active area with 8 x 8 multianode matrix with a 6 mm pixel pitch [8]. The difference from H8500 series is an higher first stage accelerating field and a revised collection geometry optimized for single photon detection [14].

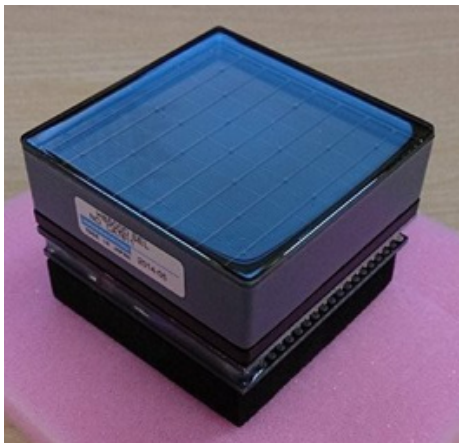

Figure 2.3: Hamamatsu H8500 MAPMT.

Figure 2.4: Hamamatsu H12700 MAPMT.

2.2 RICH Active Area

The main requirement of the RICH detector is to minimize the resolution on the Cherenkov emission angle. Focusing on the active photosensitive area, the most important elements to meet the designed performance are the number of detected photons per track and the error on the hit position, without forgetting about time precision. The error scale as

$$\sigma_{CH} = \frac{\sigma_1}{\sqrt{N}}$$

where σ_1 is the error of the single photon and N the total number of photons. The error σ_1 is related to the spatial error of the detector. The photon detector must provide a spatial resolution of less than 1 cm to not degrade the Cherenkov angle resolution.

The study in Figure 2.5 shows that, using aerogel of various refractive indexes and thicknesses, a pion-kaon separation greater than 4 sigma up to 8 GeV/c momentum can be achieved if the detector pad size is less than 1x1 cm^2 [11].

In the CLAS12 RICH, time resolution must be at the level of 1 ns, in order to be able to separate direct from reflected photons and to isolate background spurious hits. In order to meet such a resolution while reading about 25 thousands of channels, a careful calibration study is required.

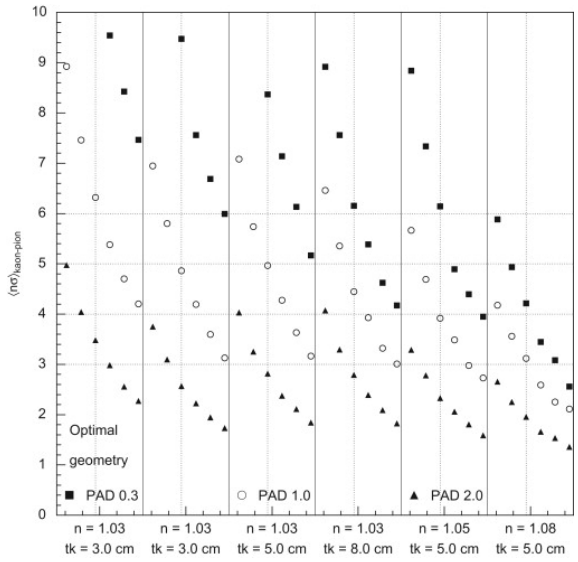

Figure 2.5: Results from MonteCarlo simulations on RICH performances. Plot of average number of sigmas in pion-kaon separation in the 5-8 GeV/c momentum range, at intervals of 0.5 GeV/c. Three photon detector pad sizes are considered (2x2, 1x1 and 0.3x0.3 cm^2), indicated by the different symbols. Various refractive indexes (from 1.03 up to 1.08) and thicknesses (from 3 up to 8 cm) of the aerogel radiator are studied as indicated on the horizontal axisv[11][12].

2.2.1 Electronic Panel

The 391 MAPMTs are organized in 138 compact units called tiles. Each of these tiles will host 2 or 3 MAPMTs depending on their position on the panel, to fully cover the trapezoidal area. In Fig. 2.6, the MAPMTs and tiles are visible and numbered respectively from 1 to 391 and from 1 to 138. Also two different colors have been used to differentiate the photodetectors types: H8500 and H12700. Each tile is composed of a stack of three boards (Fig. 2.7) [15]:

- An ADAPTER feedthrough board in the inner side of the panel to connect the MAPMTs with the electronics. It is a passive board for mechanical and electrical matching through the electronic panel with the outside of the RICH volume. It receives one high voltage power line and distributes it to groups of MAPMT.

- An Application-Specific Integrated Circuit (ASIC) board that hosts the Multi Anode Read Out Chip (MAROC). It converts the analog signals from the sensors into digitized information for the acquisition. The chip consists of 64 independent channels.

- A field-programmable gate array (FPGA) board as a controller unit. It works as a mediator to exchange the information between the front-end and the data acquisition systems. It helps configuring, controlling and debugging the front-end circuits.

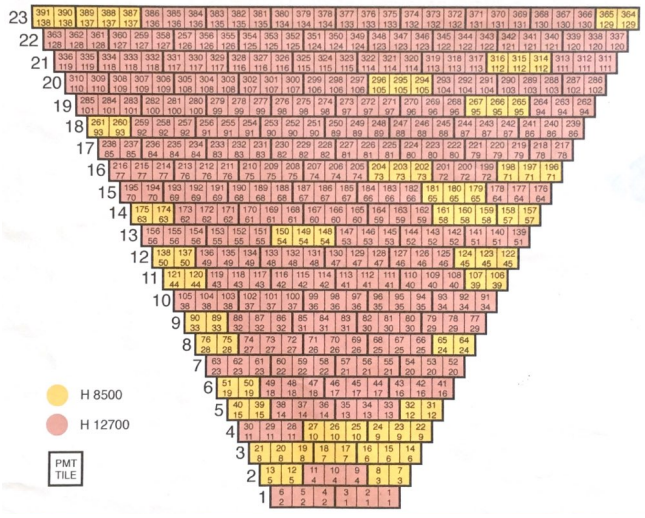

Figure 2.6: MAPMTs and tiles numbered map: H8500 and H12700 are recognized by colors.

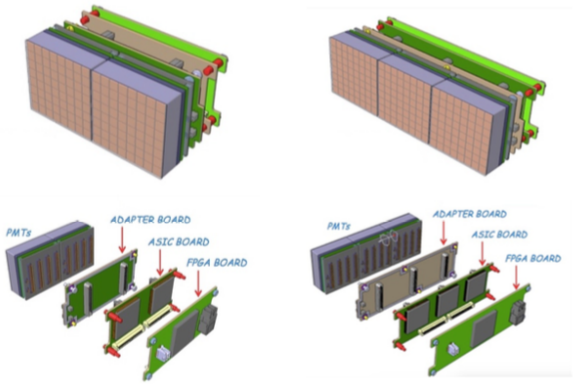

Figure 2.7: MAPMT tile assembly: electronics overview.

2.2.2 Data Acquisition

The MAROC front-end chips allow to extract analog (ADC) and digital (TDC) information for each MAPMT channel to identify the signal from a single Cherenkov photon. The analog (ADC) information provides an instantaneous measurement of the amplitude of the photoelectron signal. Being too slow for the CLAS data-acquisition, this readout mode is used only as a calibration tool. The digital (TDC) information provides a precise (1 ns precision) time measurement of the start and stop of each signal pulse.

Figure 2.8 shows a typical TDC signal behavior. The PMT pulse is amplified and shaped to a signal composed of fall edge and a rise edge. By fixing a discriminator threshold, it is possible to identify what are called start and stop times, defined as the moments when the signal crosses the threshold level. Their difference defines the duration of the pulse which is related to the recorded charge. The hit time is derived from the start time. By increasing the threshold, shorter signal duration and later start time are expected.

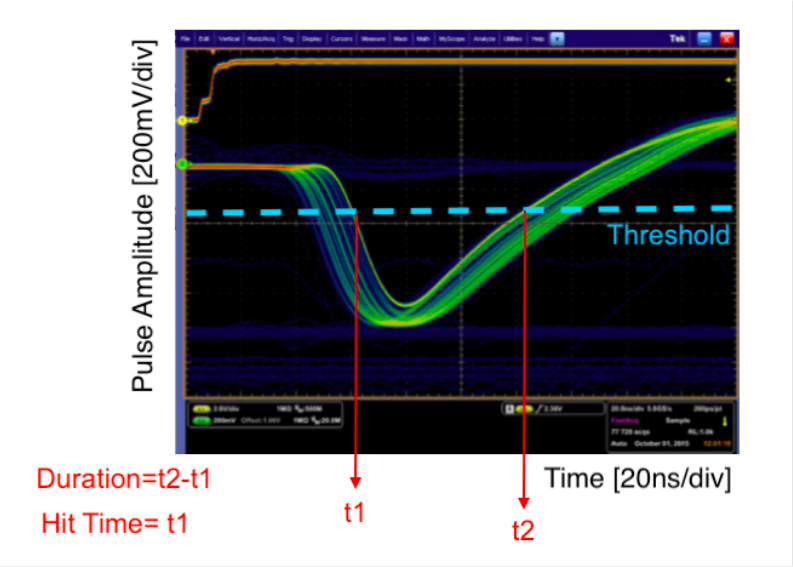

Figure 2.8: Example of TDC signal from an oscilloscope.

This type of data acquisition has two main features:

- **Time Walk** is a typical systematic effect for discriminators working at a fixed threshold. In case of two signals of different amplitudes occurring at the same time, the larger signal would cross the chosen threshold earlier than the smaller signal, causing a mismatch in the measured arrival times of the two signals. As a consequence, the measured arrival time depends (or walks) on the signal charge (duration).

- **Time Offset** is the difference in time between the discrimination of a signal and the reference clock beat. It depends on the specific length and components of each front-end circuit, but also on the distribution lines of the common clock and trigger from the central data acquisition system to the various front-end units. As a consequence it undergoes channel by channel variations of the order of few ns.

2.3 Efficiency and Performance Parameters

Performing single photon counting with a digital readout is a challenging process that requires a precise control of the PMT performance.
The most important quantity to keep in mind during this kind of work is expressed by the **detection efficiency** which is the ratio of the number of counted output pulses to the number of incident photons. It is affected by:

- Quantum efficiency of the photocatode it is the probability that the photoelectrons emitted from the cathode will impinge on the first dynode. Or, introduced differently, it is the ratio between the number of photoelectrons emitted from the photocathode with the number of incident photons per unit time (Fig.2.9).

- Collection efficiency is the probability that the photoelectrons produce a discharge on the dynodes and is related to the focalization stage of the electrodes.

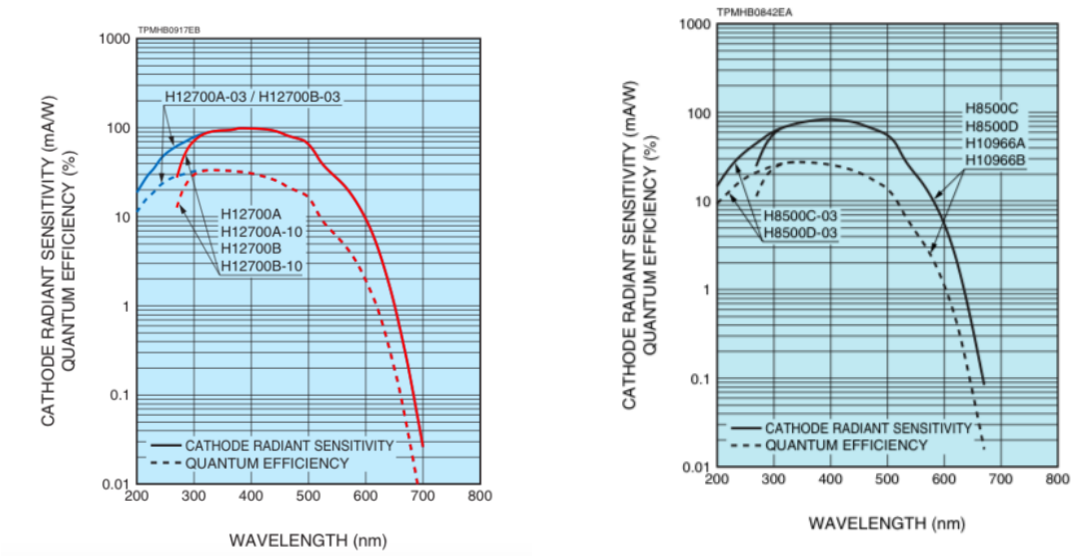

Figure 2.9: Typical Spectral Response from H8500 and H12700 MAPMTs: cathode radiant sensitivity and quantum efficiency study [7][8].

They are correlated through the following relation:

$$\text{Detection Efficiency} = \frac{N_d}{N_p} = \eta \cdot \alpha$$

where N_d are the counted pulses, N_p are the incident photons, η is the photocathode's quantum efficiency and α is the dynode's collection efficiency. They allow us to understand how the mechanical features of the device are correlated to their performance.

2.3.1 Performance Parameters

In this section a quick review of some of the main parameters that can be investigated to understand the way the photon detector works are introduced:

- **Gain** as a parameter to define the quality of the device;
- **Dark Current** to introduce the problem of the noise in these kind of sensors;
- **Crosstalk** and **Afterpulse** to show some structural problems of these technologies.

The **gain** is a parameter to define quantitatively the amount of electrons multiplication in the device after a photon strikes on the surface. The typical value for RICH's MAPMT is $3 \cdot 10^{-6}$. The difference between anode's gains change with a factor of 2 (anode uniformity [7][8]). The RICH digital readout do not require a linear response but a maximum efficiency, which means that is mainly working with saturated signals thanks to the preamplification stage of the MAROC chip.

Dark current is a source of noise: it is the current that flows inside the device even without incoming photons. It has to be kept as small as possible because it can compromise the detection and the identification of a single photon. The MAPMTs employed in the RICH have a low dark count noise, around 10-15 Hz per pixel (which means about 1kHz per MAPMT).

Crosstalk is any phenomenon by which a signal transmitted on one channel creates an undesired effect in another channel. It is usually caused by a capacitive, inductive, or conductive coupling from one readout channel to another. If the signal multiplication at the dynodes starts to broaden, it could be read out from more than one anode.

A technique used with the RICH electronics to control the crosstalk is to disentagle neighbour pixels in the MAPMTs from adjacent electronic channels. This allows to distinguish the optical crosstalk (between anodes) and the electronic crosstalk (between channels). Figure 2.10 shows a typical crosstalk study. It is a feature to be kept under control in the RICH analysis because it can influence the real signal interpretation.

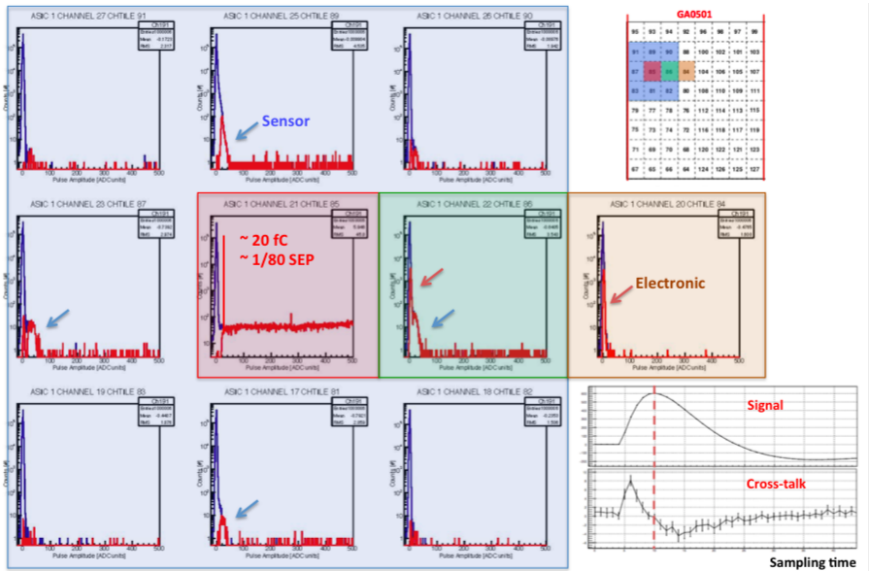

Figure 2.10: Typical signal study: electronic and optical crosstalks are analyzed.

An **afterpulse** is a spurius small amplitude signal that usually occurs later in time with respect to the main signal pulse (Fig.2.11). This kind of noise may affect low level signal measurements by causing errors in the photon (pulse) counting. This study is mainly interested on the elastic reflection of the photoelectron that would appear a few ns later than the expected signal because their probability is small (at percent level) and their effect is neglected in the following.

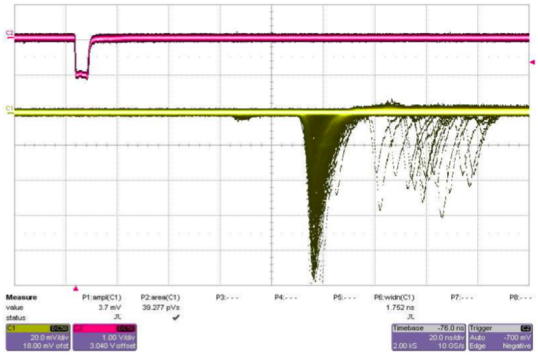

Figure 2.11: Example of afterpulses from an oscilloscope.[13]

Chapter 3

Data analysis: Time correction

This chapter is my main contribution on the RICH project. It describes a careful data analysis, focusing in particular on time correction. An explanation of the used RICH data types and features is first introduced, just followed by the main study of this thesis.

3.1 Data Analysis

The first step comprises data parsing and storage using an object-oriented program and library developed by CERN named ROOT. This software is designed for particle physics data analysis. The ROOT's tree structure allows a compact and ordered data organization and provides a C++ interface for convenient data inspection, efficient data selection and a powerful graphical interface.
The TDC individual channel data from the RICH detector are stored inside a tree structure together with the information from all the other CLAS12 detectors. This will allow a full and comprehensive data analysis of each event. The second step comprises data selection and analysis and will be the main focus of next sections.

3.2 Data variables presentation

The data variables employed for this kind of analysis have two classifications:

- **Detected variables** correspond to the data coming from the RICH readout, discussed in the previous chapter;
- **Reconstructed variables** correspond to the expected data values derived from other CLAS12 RICH detectors and a given hypothesis of particle type.

3.2.1 Detected variables

The detected variables are derived from the RICH electronic panel information. The previous chapter explained how the data is collected and stored. The two main variables are:

- **Time** is the start time of the signal at a fixed threshold, defined by the fall edge;
- **Duration** is the difference between the start and stop time of the signal at fixed threshold (defined by fall and rise edge).

All the CLAS12 detectors are synchronized by a common 250 MHz clock. The RICH FPGA generates an internal clock with a 1 ns resolution based on the common clock. The RICH detected time is defined by the FPGA clock with respect the trigger time.

The trigger signal is distributed to the CLAS12 detectors by the trigger supervisor with a precision of 4 ns, but locally processed with a 8 ns precision by the RICH FPGA. As a consequence, half of the events has a 4 ns shift that has to be corrected to align the RICH time to the CLAS12 time.

The other variables derived from RICH detection are position related. They give more details on electronic tile, MAPMT and channel number corresponding to an (x, y, z) position on the CLAS12 coordinates system.

Single fired channels are called "hits" and correspond to the Cherenkov light expected from the charged particle under study or spurious signals from several background sources (Rayleigh scattering, dark counts, cross-talks, out-of-time hits).

A group of three hits located in adjacent channels is considered a cluster. The cluster is typically related to a charged particle generating Cherenkov light on the PMT entrance window or ionization in the dynode structure. The cluster time and position are taken from the hit with longest duration. The number of hits chosen for the minimum cluster size is 3, to differentiate the cross-talk. In fact two adjacent hits are likely generated by an optical cross-talk.

Crosstalk hits are mainly recognized by the RICH reconstruction with a technique that disentangle neighbor pixels in the MAPMT's from adjacent electronic channel. This allows to distinguish the optical crosstalk (between adjacent anodes) and the electronic crosstalk (between adjacent readout channels). A further recognition is possible using properly calibrated time information.

The goal of the correction explained in this chapter therefore is to meet the design time resultion of 1 ns and to identify and reject residual cross-talk signals using such a precise time information.

3.2.2 Reconstructed variables

The reconstructed variables are the time and position expected for a given particle type that should match the RICH detector information. The reconstruction is made by using information from the CLAS12 detectors other than RICH and from a theoretical study on the Cherenkov light path. This technique is applied both for clusters and hits but with some difference.

The CLAS12 Drift Chambers and the Torus magnets give precise information on the charged particle trajectory and momentum. This allows a good reconstruction on the path inside the aerogel and the hit position at the MAPMT plane, together with the particle time of flight. The closest RICH cluster is matched to the track if the distance to the track at the PMT plane is less than 10 cm.

The reconstruction of the Cherenkov angle has been performed following the method illustrated in Fig. 3.1 which represents a top view of the RICH basic components. It exploits the information of the tracking system and of the MAPMT array and provides, for a given photon hit, the Cherenkov angle, correctly taking into account the small slope of the hadron track, of the order of few mrad, which produces a non-circular hit distribution on the MAPMT plane.

The reference frame has the z-axis along the beam line, the y-axis is vertical and pointing upwards and then $\hat{x} = \hat{y} \times \hat{z}$. The thickness of the radiator is t_{rad}, while $t_{gap} = 994$ mm and $n_{air} = 1.000273$ are the length and refractive index of the air gap between the radiator and the photodetectors.

The track enters the radiator at the point P_0 and its projection onto the MAPMT plane is P_p. Its polar and azimuthal angles are θ_p and ϕ_p, respectively.

The Cherenkov photon is emitted at the point P_c, at a depth L inside the radiator, and is detected at the point P after the refraction when exiting from the aerogel. In principle, a recursive calculation would allow a rather precise determination of L.

The point P_{pcp} is the projection of the emission point onto the MAPMT plane. The polar and azimuthal angles of the photon hit are θ and ϕ, while the Cherenkov angle, i.e. the angle between the photon direction and the track, is η_c. It is important to note that the refraction in the passage from the aerogel to the air changes its polar angle but not the azimuthal angle.

Given the small thickness of the radiators with respect to the total gap length, we assumed L = $t_{rad}/2\ tan(\theta)$.

As a result, the photon is moving on a plane and, by using the Snell equation, if the angles are known one can calculate the ring radius R as

$$R = (t_{rad} - L)tan(\theta) + t_{gap}\frac{nsin\theta}{\sqrt{n_{air}^2 - n^2 sin^2\theta}} \equiv f(\theta)$$

When the emission angle is not known but the radius R is measured, this equation must be inverted to obtain θ.

The problem is solved by minimizing the difference

$$g(\theta) = (R - f(\theta))^2$$

Once θ is obtained, the Cherenkov angle of the photon hit is given by

$$cos(\eta_c) = sin(\theta_p)sin(\theta)cos(\phi - \phi_p) + cos(\theta_p)cos(\theta)$$

Finally, the Cherenkov angle of the event, where m photon hits have been detected, is given by the average of the m Cherenkov angles.

Knowing the Cherenkov angle, one can derive also the measured refractive index of the radiator

$$n = \frac{1}{\beta cos(\eta_c)}$$

, where the velocity of the particle β is computed from the beam momentum and a given hypothesis of particle mass.

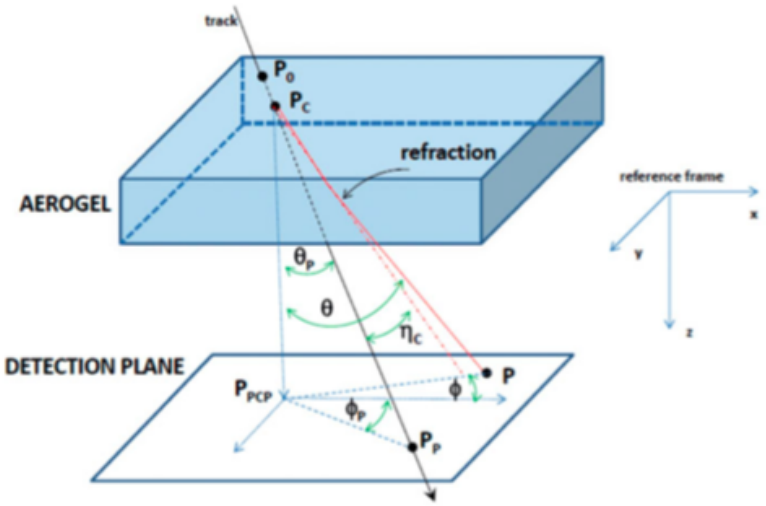

Figure 3.1: Illustration of the Cherenkov angle reconstruction [12].

At this point the single hit information detected by RICH can be matched to the information reconstructed by CLA12 and compared.

The CLAS12 event time is defined by the most precise detector, i.e. the forward TOF. The event start time is the time at the interaction point, defined as the TOF time minus the time-of-flight of the particle, once corrected to match the RF time of the beam bunches. The photon emission time is defined as the event time plus the time-of-flight of the particle at the aerogel middle point.

The reconstructed time of the photon hit is calculated by summing to the emission point the time spent by the photon in the aerogel and in the nytrogen gap before reaching the photosensors, that is extrapolated from the path suggested byminimization method. The velocity of the photon is taken to be $\frac{c}{n}$ where c is the speed of light and n the refractive index of the RICH medium (aerogel, gas).

Detected and reconstructed quantities will be studied and analyzed in the next sections.

Figures 3.2 and 3.3 show two specific events of the run 4013 at 10 GeV beam energy. Detected clusters and hits are visible in different colors. The clusters are defined in the legend with position coordinates and size, i.e. number of hits. Reconstructed and matched detected cluster positions are identified by the two crosses in the graph. RICH detector is represented by a yellow background.

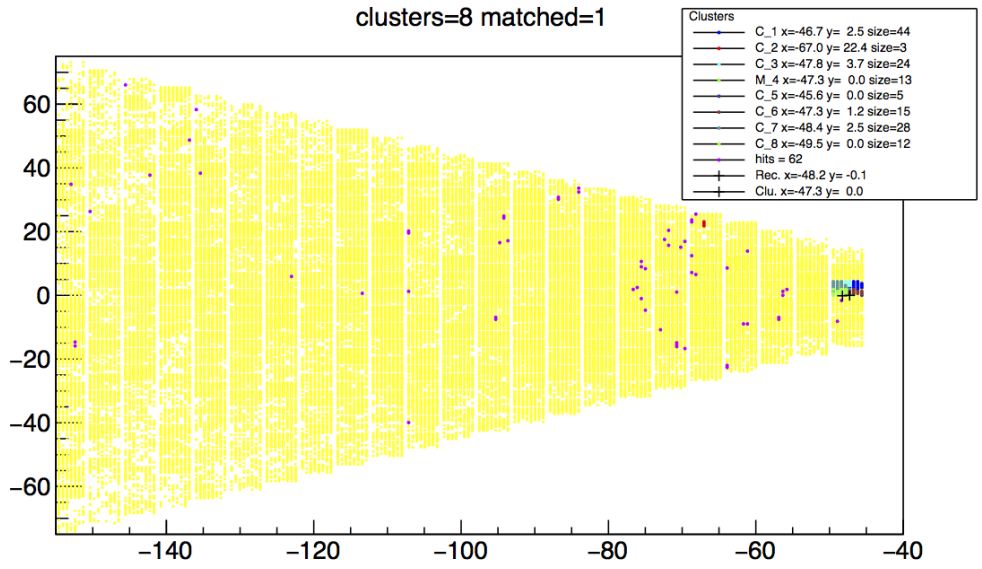

Figure 3.2: Run 4013 event 5143.

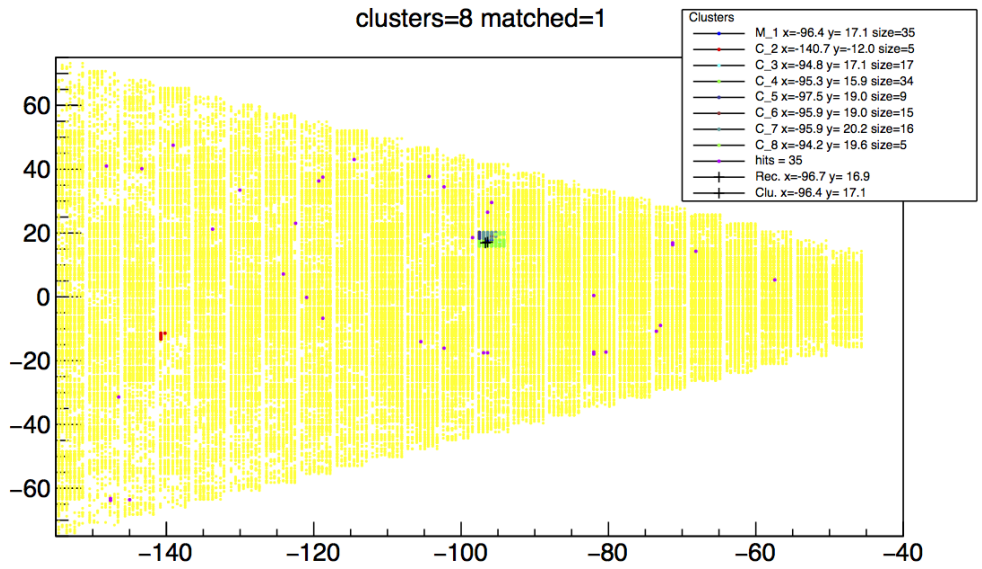

Figure 3.3: Run 4013 event 23034.

3.2.3 Probability

Reconstruction is a great tool for many aspects. In this section, it will be used to produce a quality parameter for particle identification, which is the goal of the experiment. Probabilities for electron, kaon, pion and proton hypotheses will be produced.

A probability density function is introduced to achieve this goal:

$$\text{Probability function} = \frac{e^{-\frac{(x-\mu)^2}{2\sigma^2}}}{\sqrt{2\pi\sigma^2}}$$

where x is the measured value, μ the expectation or mean and σ the standard deviation.

Cherenkov angle and time probability are defined as:

$$\text{Time probability} = A\frac{e^{-\frac{(t_m-t_r)^2}{2\sigma_t^2}}}{\sqrt{2\pi\sigma_t^2}}$$

$$\text{Angle probability} = B\frac{e^{-\frac{(\theta_r-\theta_e)^2}{2\sigma_\theta^2}}}{\sqrt{2\pi\sigma_\theta^2}}$$

where A and B are just normalization factors.

For time probability, detected t_m and reconstructed time t_r are used in the formula. They are calculated as explained in the previous sections. σ_t value before time correction should be around 20 ns, while after correction can be decreased at 1 ns.

For the Cherenkov angle probability function, reconstructed θ_r and expected θ_e angle are employed. The reconstructed angle is found during the minimization method process of the previous section. The expected angle is determined by the Cherenkov effect formula:

$$cos\theta_e = \frac{1}{\beta n}$$

where n is the nominal refractive index of the aerogel and β is calculated from the information derived from the CLAS12 drift chambers an torus magnet. The single photon angle resolution σ_θ is the one expected for the RICH, with a values of 4.2 mrad.

Cherenkov angle and time probabilities can be multiplied together to form a general probability. It will be used to test each of the four possible hypotheses: electron, kaon, pion and proton. The final particle separation will be obtained with the help of other detectors information (see Fig. 1.3).

The probability can be used for the electron control sample as a tool to determine the detection quality and to avoid any mismatch or errors in the analysis.

3.3 Duration and Time Study

Data acquisition was explained in the previous chapter, but has two features that needs to further be studied and understood:

- **Time Offset** is the difference in time between the discrimination of a signal and the reference clock beat. It depends on physical differences among the readout channel electronics but also from the central data acquisition units. Raw detected time show a channel by channel variations of the order of few ns. Fig. 3.4 shows a related time offsets study at MAPMT level.

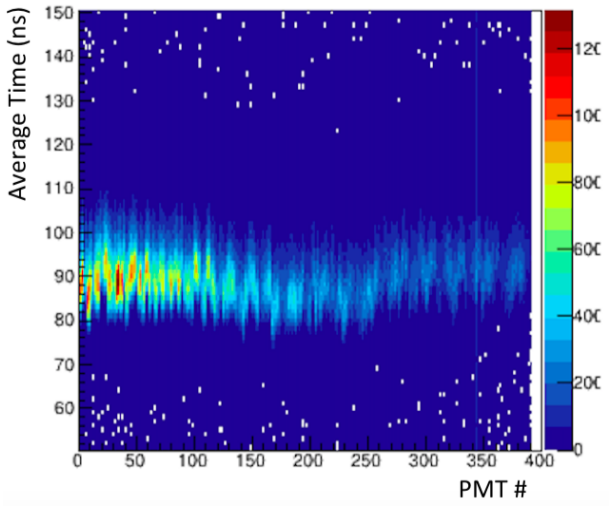

Figure 3.4: Time offsets study for each PMT.

- **Time Walk** is a typical effect for any electronics that works with a fixed threshold discriminator. The hit arrival time depends on the signal duration following the time walk.

Figure 3.5 is showing a duration-time correlation plot for the whole detector without selecting specific MAPMTs or pixels. In the following, dTime is defined as the difference between detected and reconstructed time, a quantity that should ideally average at zero with a rms smaller than 1 ns.

In the plot several important components are clearly visible:

- Cherenkov signal concentrates at dTime=0 (reconstructed and detected times match) and duration=60 (corresponding to a single saturated photo-electron signal), with a tail at smaller durations for not completely developed MAPMT discharges.
- Dark counts distribute along the vertical band at duration=60 (corresponding to a single termal-electron signal) but uncorrelated in time
- Crosstalks concentrates at small durations (small induced signal) at times later than the original saturated hit.

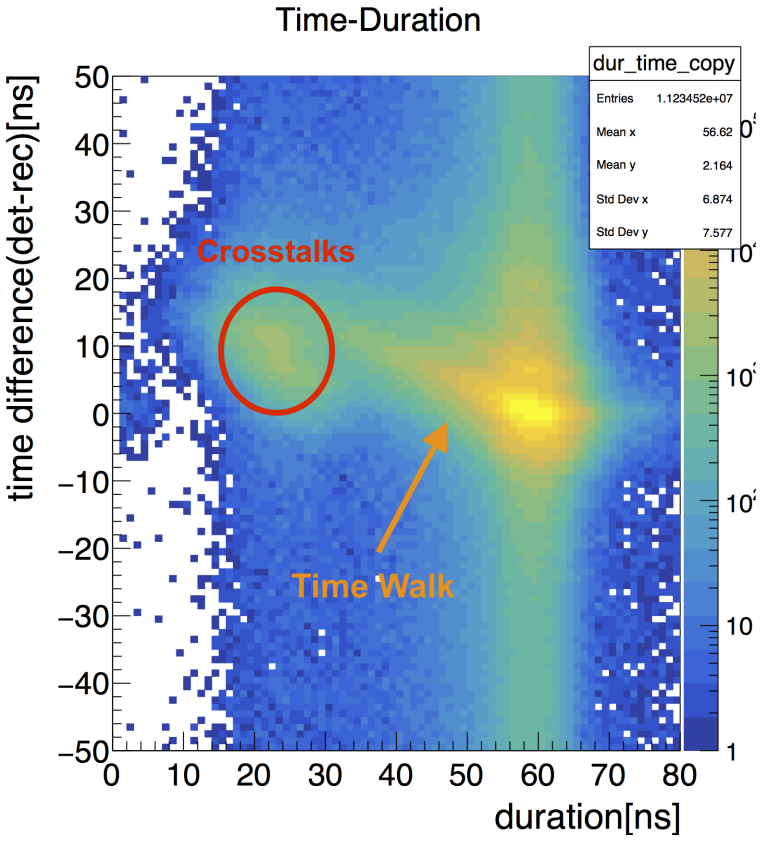

Figure 3.5: Run 4013 duration-time correlation plot before correction: crosstalks and timewalk individuation.

3.4 Time offsets

First of all, an electronic feature has to be taken into account. The RICH events are built referred to an external trigger signal, asynchronous with the CLAS12 Trigger Supervisor (TS) timestamp clock of 250 MHz. Because the trigger signal is locally processed with a 8 ns timestamp precision by the RICH DAQ, the RICH time measurements can be found shifted by 4 ns. The convention used is:

- if the TS timestamp is an even number, the detected time is accepted;
- if the TS timestamp is an odd number, 4 ns are added.

This correction has to be applied at the beginning of the study and will not be considered anymore in the next analysis.

By analyzing the difference between detected and reconstructed RICH time, it is clear that time offsets should be applied at channel level (Fig.3.6). Ideally, the dTime distribution has to be centered at 0. A channel by channel correction has to be applied to completely solve the small differences among readout circuits. In fact, an early analysis done integrating the signals over a PMT, showed a two peaks structure that was not expected. As soon as the channel by channel analysis was completed, the two peaks structure could be immediately attributed to channel's variation (Fig. 3.6). At this point, a correction file was prepared to apply the pixel by pixel offsets to the RICH time. For each

channel, the dTime value corresponding to the maximum of the time distribution is found and collected in this file. By shifting each RICH detected time by the corresponding offset, the time distribution is centered at 0 (example Fig. 3.7).

The following formula is used:

$$\Delta t = \text{(detected time + anode by anode correction) - reconstructed time}$$

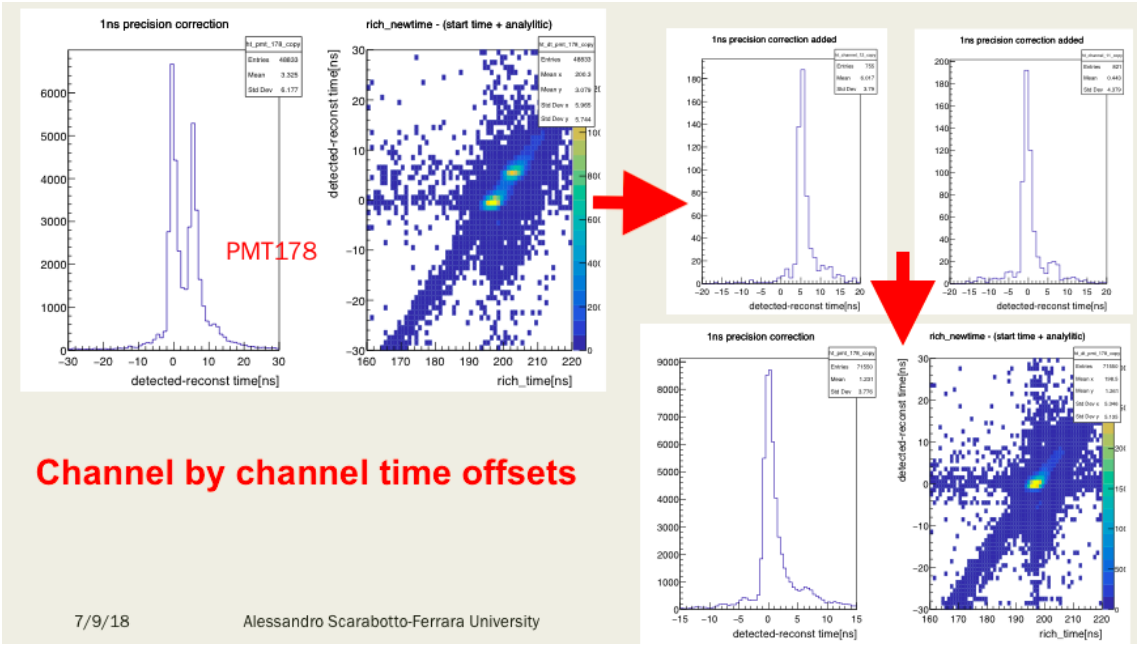

Figure 3.6: Time offsets correction procedure: the two peaks structure found on the PMT study is attributed to a channel by channel variation. The last picture shows the final correction channel dependent for the same PMT.

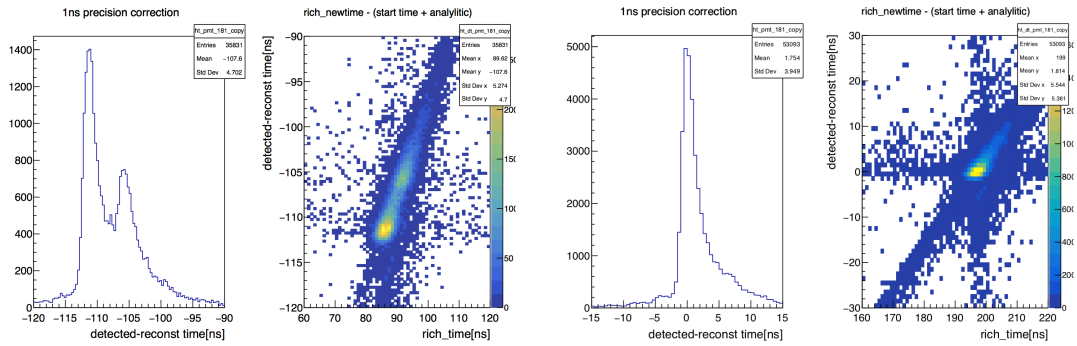

Figure 3.7: MAPMT 181: time plots before and after hits correction channel by channel.

This type of analysis can be performed considering the cluster or hit timing and their corresponding reconstruction. Figure 3.7 and 3.6 is only focused on hit correction, not considering clusters.

Figure 3.8 is showing an example of cluster related time correction. In this case, the time difference is calculated as:

$$\Delta t = (\text{detected time} + \text{offset correction}) - \frac{L}{\beta c}$$

where L is the path of the particle from the target to the RICH detector, β is the relativistic velocity relative to the speed of light c. Path and momentum are calculated by other detectors in CLAS12, mainly Drift Chambers and Time-of-Flight. The β value is derived for a given particle mass hypothesis. Without additional information, the particle is assumed to be a pion. Given the expected 1 ns time resolution, the RICH time is almost insensitive to such an assumption.

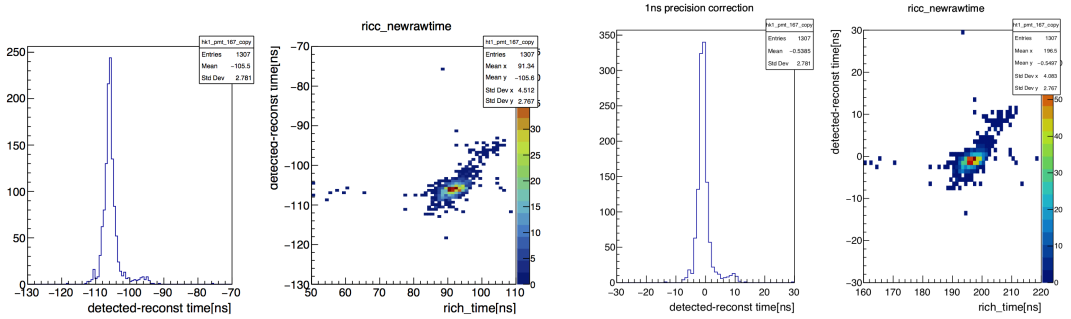

Figure 3.8: MAPMT 167: time plots before and after correction based on cluster analysis.

The offset correction has been applied to increase the precision of the RICH time measurement. The goal of this study is to obtain a correction precision better than 1 ns. The number of photon hits per event is clearly higher than the number of clusters, which allows a more complete and comprehensive time study.

The next step is to find a precise timewalk correction for the photon hits. Figure 3.9 shows how the offset time correction, that is explained in this section, is working but still not correcting the timewalk.

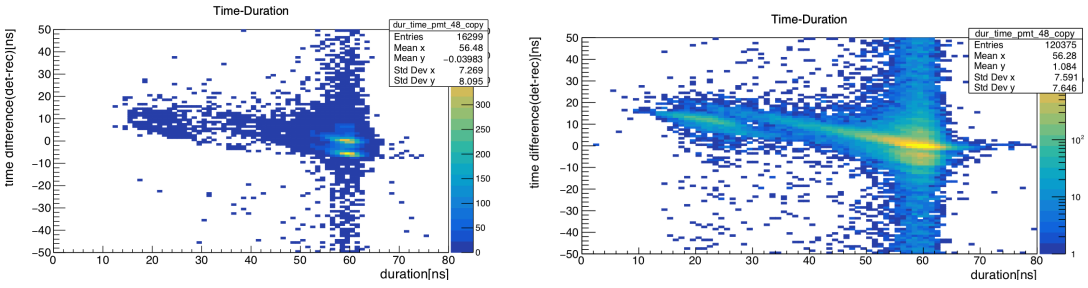

Figure 3.9: MAPMT 48: time duration plot before and after correction. The two peaks structure is finally corrected.

3.5 Time walk correction

After completing the time offset correction, the next step is to correct the time walk feature of the data acquisition. The time walk can be carefully studied and best fitted by an analytic function (Fig. 3.10).

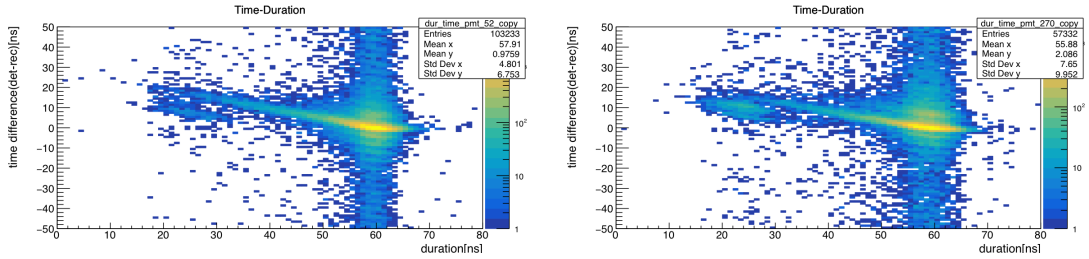

Figure 3.10: MAPMT 52 (left) and 270 (right): time duration plot before any timewalk correction: an analytic function should be chosen to best fit and correct the data.

3.5.1 Time walk fit

Different types of functions were considered to better fit the time walk: linear, exponential,... The final decision was due to the characteristics of the readout electronics. The recorded signals undergo two different regimes depending on their amplitude: non saturated and saturated. The saturation point is located around a duration of 59 ns of the hits. As a consequence, the fit function chosen for this correction was:

- a linear fit for durations between 35 ns and 59 ns for not saturated hits; the lower limit excludes crosstalk contamination.
- an independent linear fit after 59 ns duration for saturated hits.

Fig. 3.11 shows an example of such a fit.

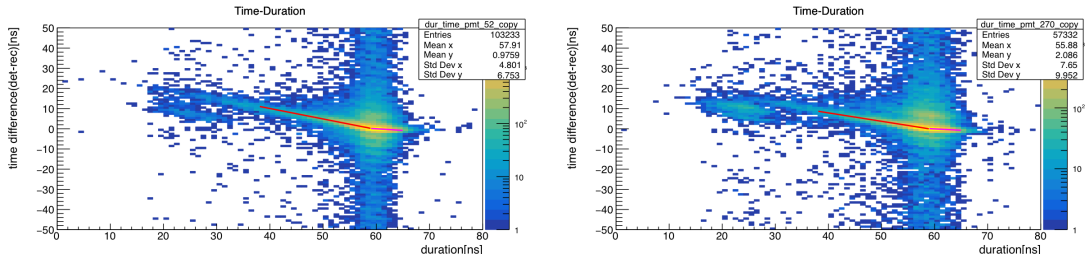

Figure 3.11: MAPMT 52 (left) and 270 (right): dTime-duration correlation plot before timewalk correction with chosen fit function: a double linear function for non saturated and saturated hits regime.

The most precise way to find these two functions is the following: the dTime-duration correlation plot is divided into 30 “slices” with 1 ns duration width in the interval of durations between 35 ns and 65 ns. The dTime distributions of these “slices” are then fitted separately with a gaussian function. Mean and sigma of the gaussian fit can be used to get precise results. The means, which correspond to the “blue dots” of figure 3.12, are plotted together with the gaussian rms as error. The error of the mean could be used instead but is probably less accurate: in fact, it assumes that dTime distributions are Gaussian, which is probably false.

Finally, by fitting the graph of means with the 2 linear fits that were explained previously, the time walk correction was found and stored.

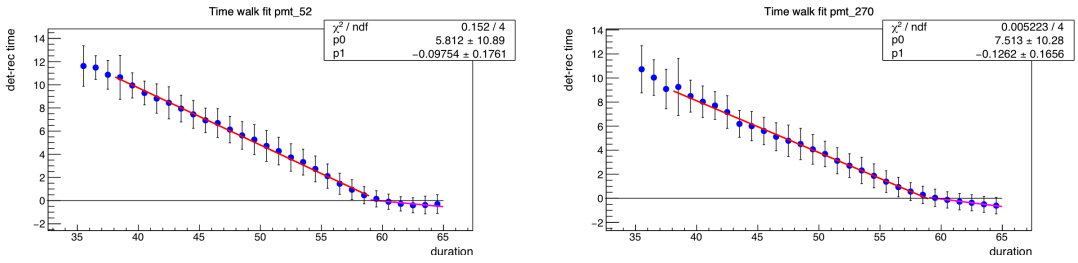

Figure 3.12: MAPMT 52 (left) and 270 (right): time walk fit function. The means of the time distribution gaussians are plotted with their sigma as an error.

The formula for the final correction is:

Δt = (detected time + anode by anode correction) - reconstructed time - timewalk correction

The "timewalk correction" is just the time value at a specific duration derived from the two linear fits. As a consequence, all the photon times shifted by the timewalk are brought back to 0, which corresponds to the expectation (Fig. 3.13).

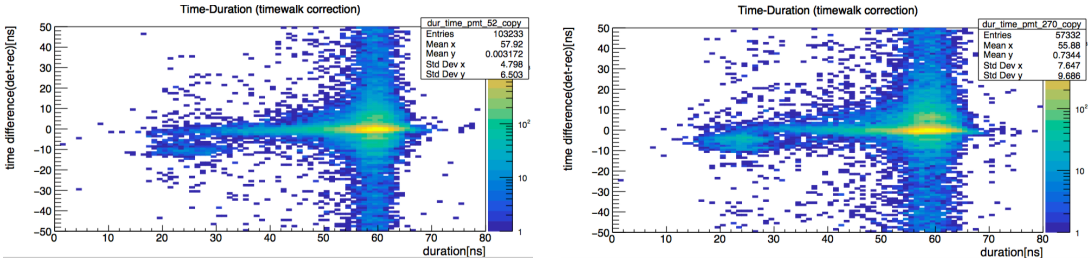

Figure 3.13: MAPMT 52 (left) and 270 (right): dTime-duration correlation plot after timewalk correction. The fitting function is analyzed and then applied to the RICH data.

3.5.2 Crosstalk cut

Most of the crosstalks are identified during the RICH reconstruction by a detection algorithm based on geometrical and amplitude criteria, the remaining ones will be corrected as explained in the next sections.

After applying offset and timewalk corrections, residual crosstalks at small durations are easily identified and removed. This technique was applied for each MAPMT: the time distribution for durations between 59 and 61 ns was found and fitted with a Gaussian function. The sigma of the Gaussian is taken as a parameter for a time cut. Finally the crosstalk rejection was done for any duration less than 40 ns at a time earlier than the average minus two sigmas of the time distribution (Fig. 3.14).

In conclusion, the crosstalk cut is completed as following:

1. A selection applied during the RICH reconstruction where hits are flagged as optical or electronic crosstalks by using geometrical and amplitude criteria (Fig.3.15).

2. A final cut based on the time information, after having applied the offset and time-walk corrections (Fig.3.16).

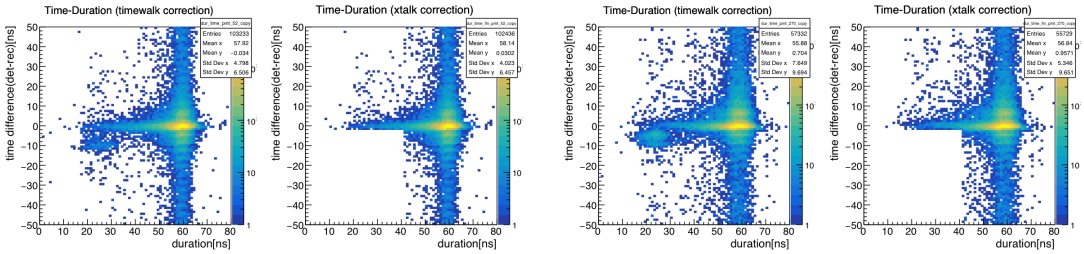

Figure 3.14: MAPMT 52 (left) and 270 (right): crosstalk cut applied after timewalk correction on dTime-duration correlation plot.

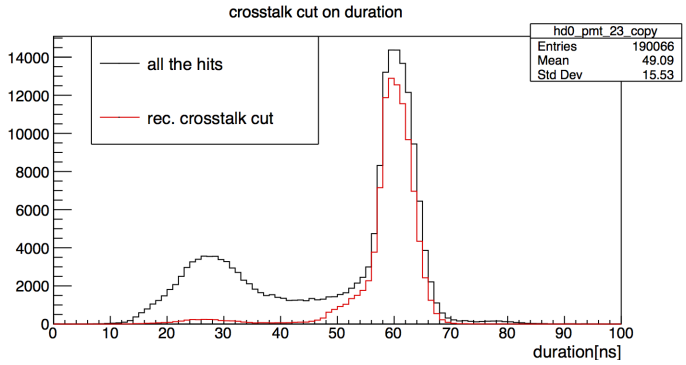

Figure 3.15: Reconstruction crosstalk selection.

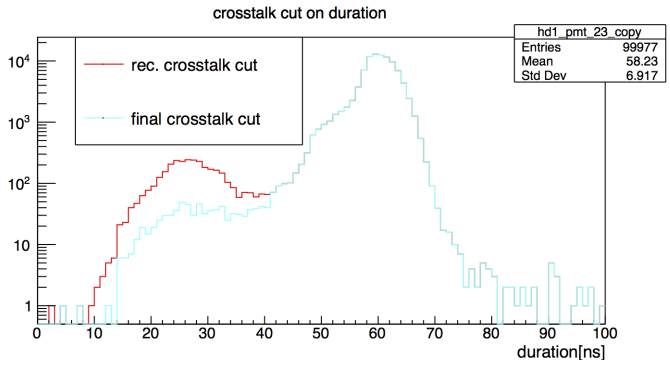

Figure 3.16: Final crosstalk rejection.

3.5.3 Time corrected distribution

Figure 3.17 is showing time plots before and after the time walk correction. It is clear that the resolution was increased. Before going into more details the study can be further refined. So far, no selection has been applied to the hits. They might correspond to either real Cherenkov photons or backgrounds. The particle identification probability can be used to enhance the sample of Cherenkov photons and get a more realistic result.

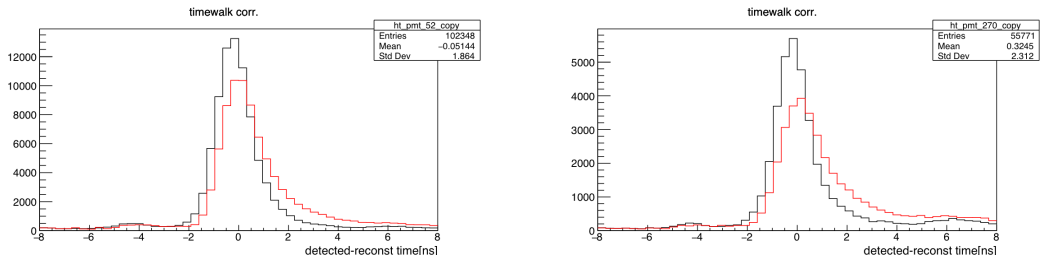

Figure 3.17: MAPMT 52 (left) and 270 (right): time plots before and after timewalk correction.

3.6 Reconstructed Photons

In this section, a more precise analysis of the RICH detected hits is investigated.

For each hit, the RICH reconstruction provides an analytically calculated Cherenkov angle and the corresponding probability for each particle hypothesis. The sample of good Cherenkov photon can be enhanced by asking a probability greater than zero, meaning a Cherenkov angle close to expectation. This sample is named "reconstructed photons" to be distinguish from "single hits" that can be either photons, crosstalks or background. This is of course causing a decrease in statistics (Fig. 3.18) but also a precision and accuracy boost.

For this particular example, pion probability greater than zero was required: at the RICH energies, pions are the dominating hadronic population and their Cherenkov signal is almost indistinguishable from the one of electron.

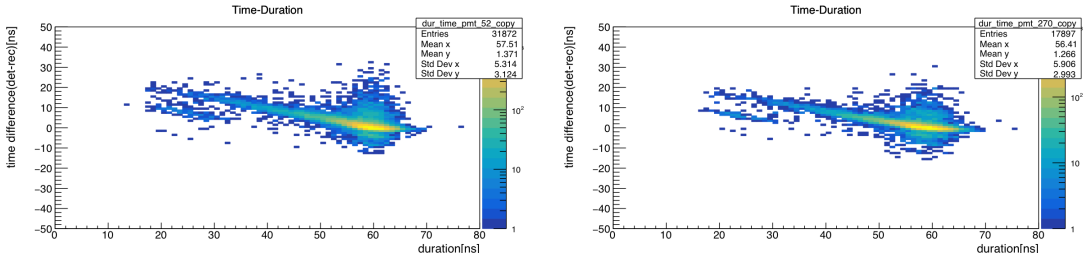

Figure 3.18: MAPMT 52 (left) and 270 (right): dTime-duration correlation plot before time calibration for reconstructed photons.

The technique used to find the time offsets and timewalk correction is the same explained in the previous sections. Figure 3.19 is showing the results.

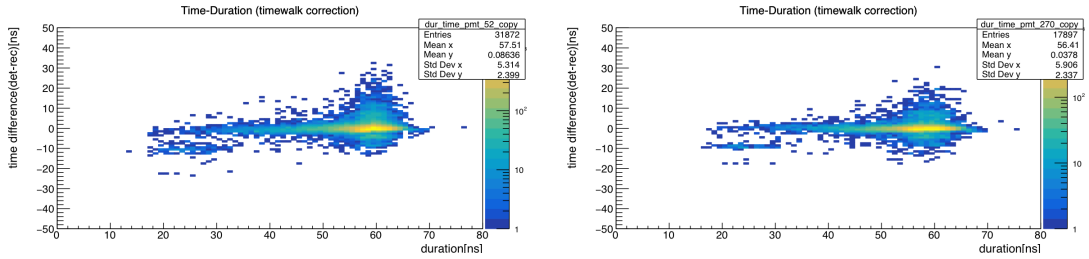

Figure 3.19: MAPMT 52 (left) and 270 (right): dTime-duration correlation plot for reconstructed photons after time calibration.

Figure 3.20 is showing the last results on time distributions. The corrected time plot is fitted with a gaussian. The resulting sigma values of the gaussian are 0.6591 ± 0.0044 for MAPMT 52 and 0.5817 ± 0.0051 for MAPMT 270. The RMS found is more accurate than the detector's specification of 1 ns. The tails seen in the figure have a 4 ns phase structure which corresponds to the beam bunch.

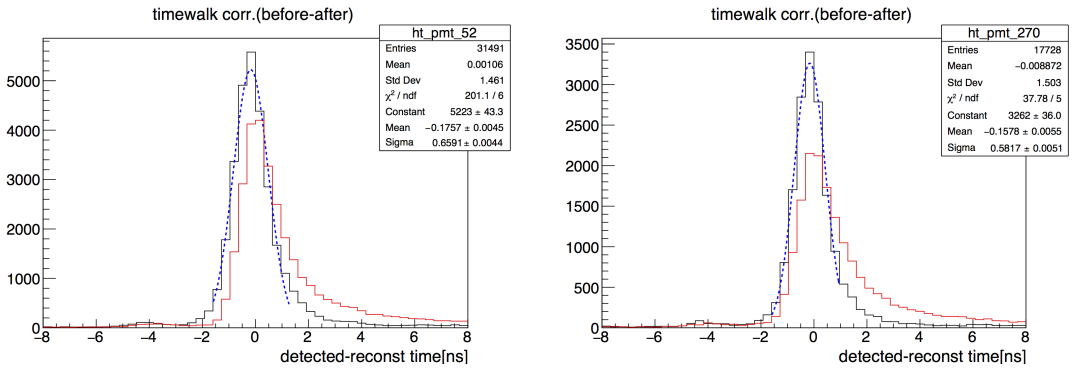

Figure 3.20: MAPMT 52 (left) and 270 (right): time distributions before and after timewalk correction for reconstructed photons.

Chapter 4

Cherenkov angle study

The time correction studied and explained in the previous chapter has an important impact on the RICH detector's performance.

The most critical parameter of a Ring Imaging Cherenkov detector is the photon's production angle. To work at single photon level is challenging not only for the small signal expected but also for the various background sources, i.e. dark counts, cross-talks and off-time hits, that can only be discriminated by time selections. The RICH design time precision of 1 ns is required to enhance the signal over background ratio and achieve the wanted angular resolution [16].

Chapter n.3 has shown how the wanted time resolution has been achieved after a detailed calibration.

Time correction also supports and improves the reconstruction. In fact, the number of reconstructed photons is greatly increased after the calibration: as shown in Chapter 2, for each charged particle the error on the Cherenkov angle scales as $\frac{\sigma_1}{\sqrt{N}}$ where σ_1 is the error of the single photon and N the total number of reconstructed photons. So by increasing the number of reconstructed photons, the Cherenkov error is decreased.

For each particle tracked by detectors other than RICH, the mean Cherenkov angle can be calculated as the average over all the reconstructed photons. The RMS of this distribution defines the angle resolution of the detector. By improving the angle resolution, the confidence on the particle ID is increased.

In this chapter, probabilities explained in section 3.2.3 will be discussed and analyzed. After applying the time calibration, angle and time probabilities can be used to study the RICH performance in Cherenkov angle resolution.

4.1 Electron Cherenkov light production

As a basic test sample, particles identified as electrons will be studied. In fact, other CLAS12 detectors have already a very good electron identification. RICH is not intended to identify electrons. Particles identified by CLAS12 detectors other than the RICH represent an independent control sample useful to estimate the RICH performance.

This analysis will be used as a reference for later studies on Pion-Kaon particle identification, which is the main goal of the RICH detector.

4.1.1 Single photons Analysis

Initially, single photon time probability is analyzed. The time information could be used as a quality estimator of the reconstructed photons, after applying a very loose selection simply asking for an electron angle probability greater than zero.

Figure 4.1 shows the time probability distribution. A probability cut of 0.03 is applied to reject out of time hits that likely come from close but different beam bunches.

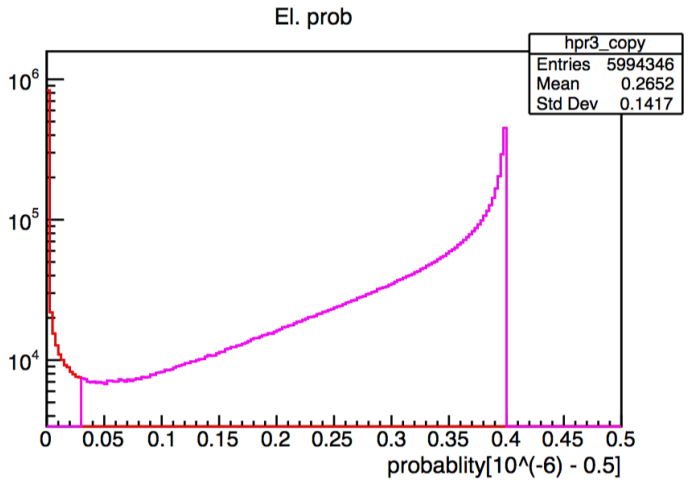

Figure 4.1: Electron time probability distribution after time calibration.

Figure 4.2 compares the Cherenkov angle distribution before and after the selection in time probability. The selection is rejecting most of bad reconstructed photons that populate mainly the tails of the distribution as represented by the red plot.

After the time probability selection, the RMS of a gaussian fit of the Cherenkov angle distribution is 0.35 degree which is close to the RICH goal single photon angle resolution of 4.5 mrad.

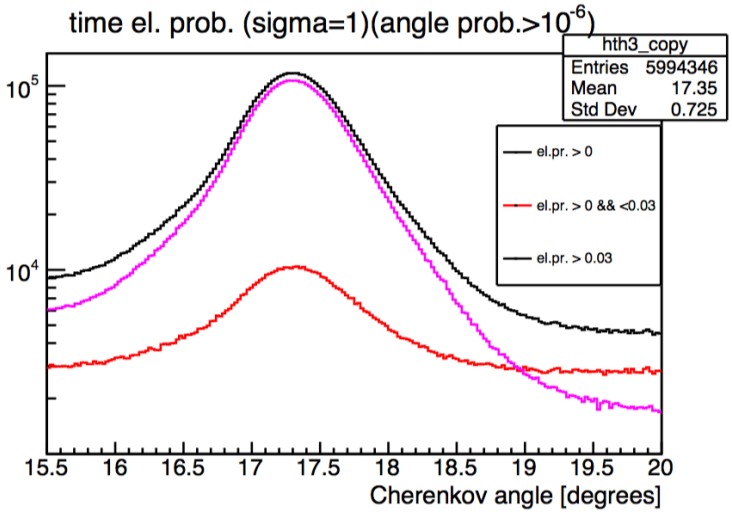

Figure 4.2: Cherenkov angle's distributions: the black plot represents the full hits distribution while the magenta shows a sample selected by the time probability cut. The red graph is the difference of the other two distributions and represents the badly reconstructed hits.

The Cherenkov angle is in principle dependent on the momentum of the electron. The light blue line on Fig. 4.3 represents the expected value of the angle for different momenta and indicates that the Cherenkov angle of electrons is always saturated in the RICH interval of momenta. The reconstructed values on the plot are coherent with the expectations of a saturated ring but all shifted down by approximately half a degree. This problem can be attributed to a systematic error on the detector, i.e. a misalignment.

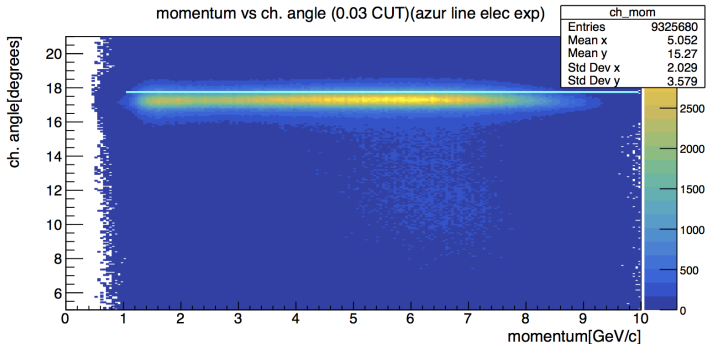

Figure 4.3: Cherenkov angle vs momentum correlation plot for particle identified as electrons by CLAS12. The light blue line represents the electron's Cherenkov angle expected.

4.1.2 Time Calibration Effects on Reconstruction

This study will also evaluate the time calibration, explained in the previous chapter, effectiveness.

Figure 4.4 shows the Cherenkov angle distribution before and after time correction. Time calibration is increasing effectively the number of reconstructed photons. This is a very important result. In fact the time error for each hadron scales as $\frac{\sigma_1}{\sqrt{N}}$, as explained at the beginning of the chapter. From the figure, the number of reconstructed photons is

increased by a factor of 10 after time calibration, which means that the Cherenkov error is greatly decreased.

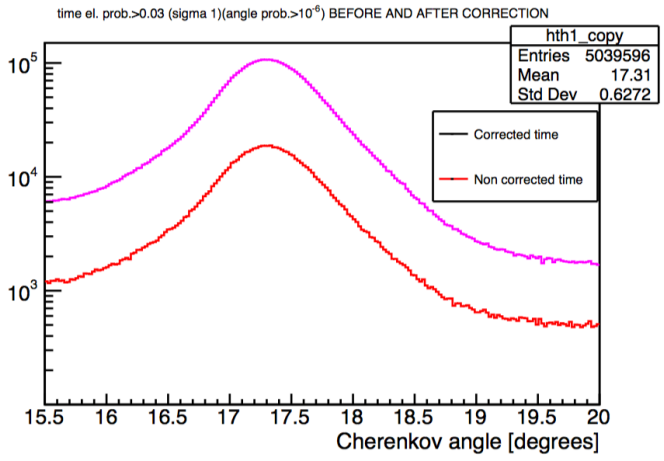

Figure 4.4: Cherenkov angle distributions before and after time calibration.

Another important achievement of the time correction study is the residual crosstalk rejection.

Figure 4.5 shows the Cherenkov angle distribution for crosstalks identified by the time criterium compared with the reconstructed photons. The RMS of a gaussian fit of the crosstalk distribution is 0.6 degrees. The time calibration allows to reject the undesired crosstalks hits whose angular distribution has a sigma greater than the photon distribution

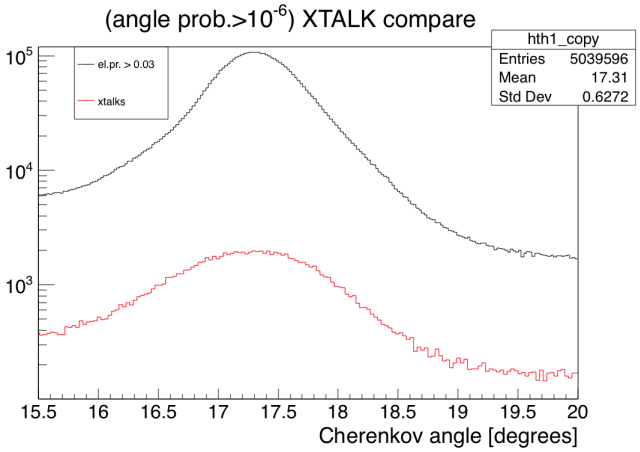

Figure 4.5: Cherenkov angle distributions study for crosstalk selection.

4.1.3 Mean Cherenkov angle

In this section, the mean Cherenkov angle is calculated by summing all the angles of reconstructed photons produced by the same particle and dividing it by the number of reconstructed photons. In this way, the angle resolution eventually entering the PID selection can be discussed.

Figure 4.6 shows the mean Cherenkov angle distribution from each electron tracked by detectors other than RICH with at least 5 reconstructed photons. The resulting angle resolution, estimated as the RMS of a gaussian fit, is 0.24 degrees, which is better than the single photons plot but is not satisfying the expectations of 0.08 degrees [16].

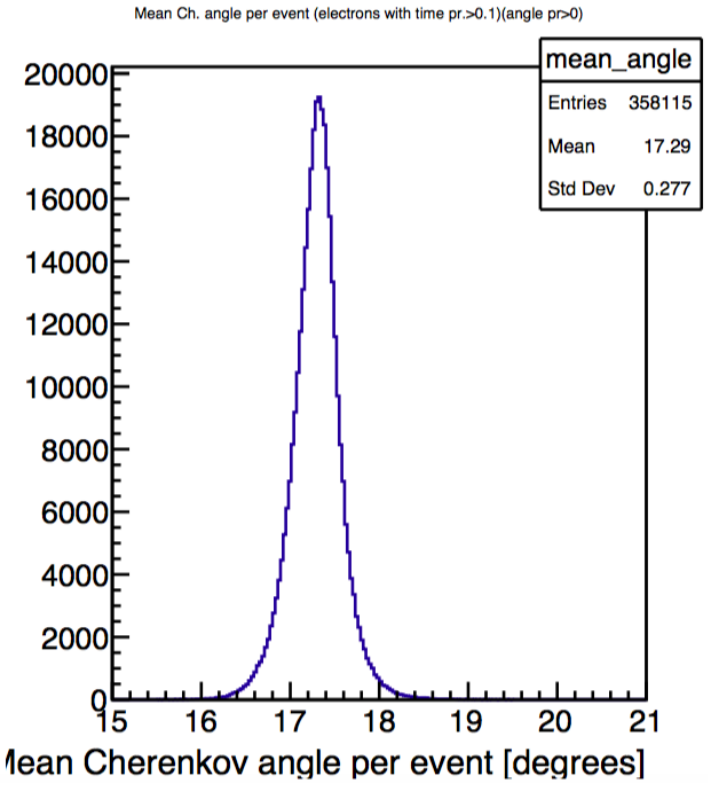

Figure 4.6: Mean Cherenkov angle distributions study per event.

Some problems in this analysis were accounted and studied as follows.

The number of reconstructed photons per event is not equally distributed over the detector aerogel surface (see Fig. 4.7). In fact, the RICH data is not yet taking into account any reflected photons from the mirrors. In the central part of the detector, the whole Cherenkov ring is reconstructed because the photons are imaged directly without any reflection. The average number of 18 is consistent with the TDR [16] expectations. At the RICH borders, the number of reconstructed photons is limited because a large fraction is reflected and, at the moment, not reconstructed.

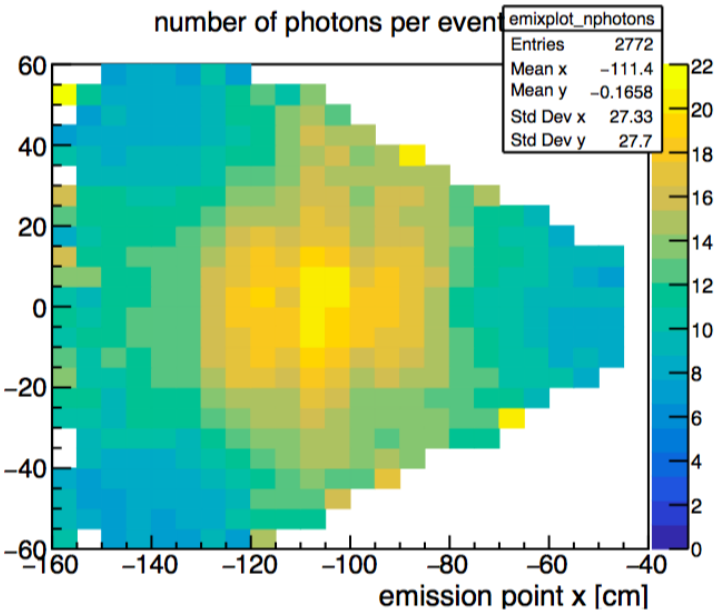

Figure 4.7: Number of reconstructed photons per event as a function of the photon emission point in the aerogel.

The mean Cherenkov angle per event is studied as a function of the electron's Cherenkov light emission point in the aerogel. Figure 4.8 shows not homogenous values of the angle at different emission positions. The Cherenkov effect, as explained in the first chapter, depends on the refractive index of the radiator that is here taken at the nominal value of 1.05. These differences in the plot can be attributed to small discrepancies on the real refractive indexes of the various aerogel tiles which is causing local Cherenkov angle's variations. The solution of the above limitations, required to achieve the wanted RICH resolution, is in progress but goes beyond the scope of this work.

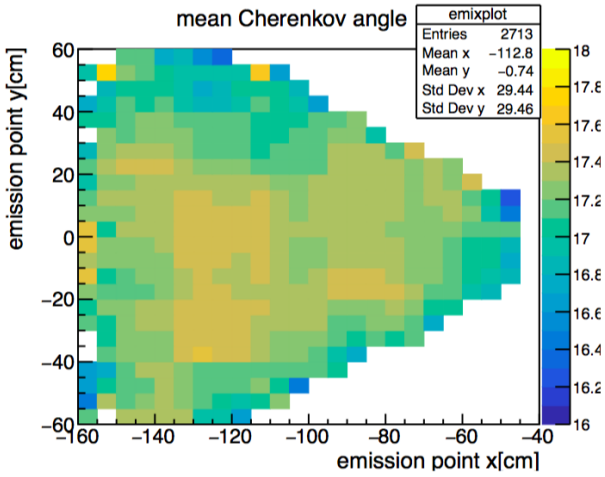

Figure 4.8: Mean Cherenkov angle per event as a function of the photon emission point in the aerogel.

Conclusions

Ferrara physics research teams are committed to provide a strong contribution and continuous improvements to technology solutions in support to subatomic particle detection experimentation.

The RICH detector has been specifically developed under the lead of Ferrara researchers, to access quark flavor decomposition in various deep inelastic experiments at Jefferson Lab.

The detector working principle is based on Cherenkov light photosensors and electronics able to reach single photon sensitivity.

In spring 2018 I joined the Ferrara research group at the JLAB in Virginia. I was given the unique opportunity to have a live experience at the JLAB Experimental Hall B where the new RICH detector has been recently integrated into the large acceptance CLAS12 spectrometer.

I supported the group in the crucial effort to analyze the data collected by the RICH detector, after being integrated in CLAS12 and used for the first time in actual physics runs.

The RICH detector comprises 25000 independent pixels covering an area of about 1 squared meter and a digital readout that only record the hit start time and duration of active channels.

The main focus of this work was on time correction study and application on RICH detected data. The analysis was based on the RICH reconstruction that is a necessary and powerful tool used to compare the detected information with the theoretical expectations.

The time correction study has been conducted in two steps: time offset correction at channel level and time walk correction at sensor level. The second was done using two different linear fits for non saturated and saturated hits. The time resolution found after the correction is less than 1 ns, i.e. 0.7 ns, which fully met the expectations, and also allowed an almost complete crosstalk rejection.

The RICH time precision of less than 1 ns is required to enhance the signal over background ratio and achieve the wanted Cherenkov angular resolution. By improving the angle precision, the confidence on the particle ID is eventually increased.

After the time calibration, the number of reconstructed photons for a full Cherenkov ring approaches the TDR value of 18 and the resulting single-photon angle resolution found is 0.35 degrees, which is close to the RICH design specification of 0.24 degrees. This lack in resolution is caused by small discrepancies of the real refractive indexes of the various

aerogel tiles with respect the adopted nominal value of 1.05. This reflects in a still limited average Cherenkov angle resolution per hadron track of 0.24 degrees. The solution of the above limitations, required to achieve the wanted RICH resolution, is in progress.

The outcome of this analysis is leading to a confirmation of design RICH performance and to the installation of a second RICH detector replacing another LTCC detector. The implementation of this PID capability will ensure a significant improvement in precision and effectiveness on any further CLAS12 experimental study.

JLAB CLAS12 performance improvements are part of the continuous technology development in Nuclear and High Energy physics research, which ultimately will contribute to the progress in our knowledge of the atomic and subatomic world.

Bibliography

[1] Department of Energy Laboratory Plan -TJNAF, June 30, 2017, https://www.jlab.org/media_relations/JLAB_10_year_plan_public.pdf

[2] R D McKeown 2011 J. Phys.: Conf. Ser. 312 032014, "The Jefferson Lab 12 GeV Upgrade of the CLAS12 experiment"

[3] "Thomas Jefferson National Accelerator Facility", https://arxiv.org/pdf/1208.1244.pdf

[4] The CLAS12 Detector, https://www.jlab.org/Hall-B/clas12-web/subsystems/CLAS12-Detector-overview.pdf

[5] "Chapter 2: Basic principles of photomultiplier tubes", https://www.hamamatsu.com/resources/pdf/etd/PMT_handbook_v3aE-Chapter2.pdf

[6] "Chapter 9: Position sensitive photomultiplier tubes", https://www.hamamatsu.com/resources/pdf/etd/PMT_handbook_v3aE-Chapter9.pdf

[7] Hamamatsu H8500 Series Flat Panel Type Multinanode PMT Assembly: https://www.hamamatsu.com/resources/pdf/etd/H8500_H10966_TPMH1327E.pdf

[8] Hamamatsu H12700 Series Flat Panel Type Multinanode PMT Assembly: https://www.hamamatsu.com/resources/pdf/etd/H12700_TPMH1348E.pdf

[9] J.Eschkea, C.Hhnea, Nuclear Instruments and Methods in Physics Research Section A: Accelerators, Spectrometers, Detectors and Associated Equipment, Vol: 639, Publication Year: 2011 , Page: 307-310

[10] R.A. Montgomery et al., Nuclear Instruments and Methods in Physics Research Section A: Accelerators, Spectrometers, Detectors and Associated Equipment, Vol: 790, Publication Year: 2015 , Page: 28

[11] M. Contalbrigo et al., Nuclear Instruments and Methods in Physics Research Section A: Accelerators, Spectrometers, Detectors and Associated Equipment, Vol: 639, Publication Year: 2011 Page: 302

[12] Anefalos Pereira, S., Baltzell, N., Barion, L. et al. Eur. Phys. J. A (2016) 52: 23. https://doi.org/10.1140/epja/i2016-16023-4

[13] M. Turisini (pag. 56-57) http://www.roma1.infn.it/exp/nemo/AHEN/Thesis/Turisini_Tesi_Specialistica.pd

[14] I. Balossino, "Studies of innovative photon detectors working in the single-photon regime for the RICH detector"

[15] M. Turisini, "The CLAS12 RICH readout electronics: design, development and test"

[16] "CLAS12 RICH Technical Design Report", 2013, http://www.lnf.infn.it/ mirazita/RICH/RICH_TDR.pdf